Long-range GABAergic projections contribute to cortical feedback control of sensory processing

Camille Mazo, Soham Saha, Antoine Nissant, Enzo Peroni, Pierre-Marie Lledo, Gabriel Lepousez

Long-range GABAergic projections contribute to cortical feedback control of sensory processing.

Camille Mazo[1,2,*], Soham Saha[1], Antoine Nissant[1], Enzo Peroni[1], Pierre-Marie Lledo[1,#] and Gabriel Lepousez[1,#,*]

[1] Laboratory for *Perception and Memory*, Institut Pasteur, F-75015 Paris, France; Centre National de la Recherche Scientifique (CNRS), Unité Mixte de Recherche (UMR-3571), F-75015 Paris, France.

* Corresponding authors to whom correspondence should be addressed:

Laboratory for Perception and Memory, Institut Pasteur, 25 rue du Dr. Roux, 75 724 Paris Cedex 15, France. **Tel**: (33) 1 45 68 95 23

E-mail: gabriel.lepousez@pasteur.fr

E-mail: camille.mazo@gmail.com

[#] Jointly supervised this work

[2] now at Champalimaud Research, Champalimaud Center for the Unknown, Lisbon, Portugal

Keywords: Sensory circuits, Top-down, Inhibitory, Centrifugal, Olfactory system, Barrel cortex

Abstract

In sensory systems, cortical areas send excitatory projections back to subcortical areas to dynamically adjust sensory processing. Here, we uncover for the first time the existence of a cortical inhibitory feedback to subcortical sensory areas. Investigating the olfactory system, we reveal that a subpopulation of GABAergic neurons in the anterior olfactory cortex target the olfactory bulb. Analogous inhibitory cortico-thalamic projections were also present in the somatosensory system. Long-range inhibitory inputs synapsed with both local and output neurons of the olfactory bulb. At the functional level, optogenetic activation of cortical GABAergic projections caused a net subtractive inhibition of both spontaneous and odor-evoked activity in local as well as output projection neurons, mitral and tufted cells. In tufted cells, but not mitral cells, this resulted in an enhanced separation of population odor responses. Furthermore, GABAergic corticofugal projections entrained network oscillations in the communication band between the cortex and the olfactory bulb. Targeted pharmacogenetic silencing of the cortical GABAergic outputs in the olfactory bulb impaired discrimination of similar odor mixtures. Thus, cortical GABAergic feedback represents a new circuit motif in sensory systems involved in refining sensory processing and perception.

Introduction

Long-range GABAergic projection neurons in the brain have been described for over a century in the cerebellum (Purkinje cells) and striatum (medium spiny neurons) where they constitute the main output of their structure. With the development of single-cell tracing, it is only towards the end of last century that anecdotal reports of these GABAergic projection neurons in the cortex were described[1–3]. Nowadays, advanced genetic tools applied to cell- and circuit-tracing has allowed for the discovery of a significant variety of long-range GABAergic projection neurons in the cortex – where they may constitute 1-10% of the total GABAergic neurons in mice, rats, cats and monkeys[4–8]. They express predominantly somatostatin (SOM) and neuronal nitric oxide synthase 1 (nNOS1)[9–13], but can also express parvalbumin (PV)[14–17], and more rarely the vasoactive intestinal peptide (VIP)[18]. PV- and SOM-expressing long-range projecting neurons have been found to be intermingled within a single structure, where they exhibit distinct connectivity and exert various functions[19]. For instance, bidirectional GABAergic projections between the hippocampus and entorhinal cortex synchronize the rhythmic network activity and gate spike-timing plasticity[11,20], cortico-striatal and cortico-amygdala GABAergic projections regulate spike generation and excitability of their postsynaptic target[21,22] and influence locomotion as well as reward coding[15,19]. VIP^+ GABAergic projection neurons of the hippocampus were also found to be differentially recruited during different brain states[18].

In sensory systems, external stimuli trigger a feedforward flow of information from the sensory organ to the primary and higher-order sensory cortices via a set of subcortical structures, thereby defining a hierarchy between sensory brain regions. In parallel, higher-order cortical sensory areas send top-down information to lower-order areas, constantly shaping information processing. Such feedback is thought to convey contextual information and predictions to lower areas, not only playing a decisive role in selective attention and object expectation, but also in the encoding and recall of learned information[23,24]. Long-range cortical projections are thought to be mediated by glutamatergic neurons, while GABAergic neurons

are in turn frequently referred to as exclusively mediating local information processing[25] (but see[26,27]). In the present study, we challenge that view by investigating whether sensory cortical circuits can also parallelize excitatory and inhibitory top-down projections.

In the olfactory system, sensory neurons project to the external layer of the olfactory bulb (OB; the glomerular layer, GL), where the signal is transmitted to mitral and tufted cells (MCs and TCs, respectively), the output projection neurons of the OB. MC and TC activity is shaped by a large population of local GABAergic interneurons which synapse onto their apical or lateral dendrites. The anterior olfactory nucleus (AON) and the anterior piriform cortex (APC) —forming the anterior olfactory cortex (AOC) — is the primary recipient of OB outputs. Similar to the cortico-thalamic feedback pathway, the AOC send extensive projections back to the OB[28,29,38,30–37]. Glutamatergic feedback projections from the AOC target virtually all types of neurons in the OB and induce robust disynaptic inhibition onto MCs and TCs[35,36,39–41]. These reciprocal connections between the OB network and the AOC are important for proper oscillations in the OB[42,43], decorrelation of OB output activity[44], inter-hemispheric coordination[45] and may modulate odor perception threshold[46] and odor-association learning[47] in a context-dependent manner[48].

Here we reveal that in addition to the glutamatergic feedback, the AOC sends GABAergic projections back to the OB. In particular, the AON *pars posterioralis* (AONp) formed a particularly dense cluster of OB-projecting GABAergic neurons. Similar to their glutamatergic counterpart[35,36], we demonstrate that cortical GABAergic feedback forms synapses with MCs, TCs and with deep-layer GABAergic interneurons, but spares GL GABAergic neurons. *In vivo*, we found that GABAergic feedback drives a net inhibition of both spontaneous and odor-evoked activity in both local and output neurons, and participated in the entrainment of specific network oscillations in the OB. At the behavioral level, silencing of cortical GABAergic projections impaired fine odor discrimination of close binary mixture of enantiomers. Lastly, cortico-subcortical GABAergic projections were also observed between the primary somatosensory cortex (S1) and its respective lower-order thalamic nuclei. Collectively, our study shows

cortical GABAergic feedback could be a prominent motif in sensory circuits important for sculpting the integration of sensory inputs.

Results

Anterior olfactory cortex sends GABAergic projections to the OB

To determine whether the AOC sends GABAergic projections back to the OB, in parallel to the well-described glutamatergic projections, we expressed different fluorescent reporters in the GABAergic and glutamatergic populations of the AOC. In VGAT-Cre mice, we employed conditional genetics approach to restrict expression of eYFP in GABAergic neurons while mCherry was expressed in excitatory neurons using the CaMKIIa promoter (Extended Data Fig. 1a,c). We ensured that eYFP axons were *bona fide* GABAergic as expression of GABA synthesizing enzymes (Glutamic Acid Decarboxylase 65/67, GAD65/67; Extended Data Fig. 1b) were observed by immunostaining. GABAergic and glutamatergic axons intermingled in the OB and, in contrast to glutamatergic projections, GABAergic projections were strictly ipsilateral. To directly compare the OB innervation patterns by GABAergic projections from the olfactory cortex vs from the nucleus of the diagonal band and magnocellular preoptic area (NDB/MCPO)[49–55], we virally labeled them with different fluorescent reporters (**Fig. 1a**). Cortical and basal forebrain GABAergic axons were both found in the OB but did not colocalize (**Fig. 1b,c**), ruling out possibilities of cross-diffusion of the virus. Moreover, NDB/MCPO and AOC axons exhibited distinct innervation patterns across OB layers. The granule cell layer (GCL), internal plexiform layer (IPL) and Mitral Cell layer (MCL) were common targets of both projections. In contrast, NDB/MCPO projections targeted the entire glomerular layer (GL) and the internal part of the external plexiform layer (EPL), while AON/APC projections were scarce in these layers, and restricted to the internal part in the GL (**Fig. 1b,c**).

We next wondered whether such inhibitory cortical feedback to subcortical structures also existed in other sensory systems. In S1, we performed a dual anterograde labeling of deep GABAergic and glutamatergic neurons (**Fig. 1d**). GABAergic axons were found alongside glutamatergic axons in the lower-order (ventroposterior medial and lateral, VPM and VPL) and higher-order (posteriomedial, POm) somatosensory thalamic nuclei (**Fig. 1e**). GABAergic cortico-thalamic projections intermingled with

glutamatergic projections and did not seem to project to other thalamic territories. Altogether, these results indicated that GABAergic neurons in primary sensory cortices provide extrinsic inhibition to subcortical sensory areas.

Neurochemical identity of the long-range GABAergic projections to the OB.

We next employed a conditional retrograde labeling approach to identify the sources of cortical GABAergic feedback to the OB. A Herpes Simplex Virus (HSV) expressing GCaMP6f in a Cre-dependent manner was injected unilaterally in the OB of VGAT-Cre mice (**Fig. 2a**). Retrogradely labeled cells were found in the ipsi-lateral, but not contra-lateral side of the injection, confirming our earlier observations. Retrogradely-labeled cells were found mainly in the AON, APC and NDB/MCPO, and occasionally in the posterior piriform cortex (PPC) and tenia tecta (TT), but not in the olfactory tubercle (OT) — a large striatal GABAergic structure of the olfactory system (**Fig. 2a-c**, Extended Data Fig. 1d). Retrogradely-labeled cells were not uniformly distributed within the AOC. Roughly two-third of the labelled cells being concentrated in the AON *pars posterioralis* (AONp) — the most caudal part of the AON, located in between the APC and the OT (**Fig. 2c**). An appreciable fiber tract was often observed between the AONp and the NDB/MCPO (**Fig. 2a**), yet the newly identified cluster of GABAergic projection neurons was not a rostral extension of striatal or pallidal territory as it did not contain neurons expressing the acetylcholine-synthesizing enzyme ChAT– in contrast to the OT and NDB/MCPO (Extended Data Fig. 1f). To confirm these observations based on viral retrograde vectors, we labeled OB-projecting neurons using a classical chemical retrograde tracer (cholera toxin subunit-B conjugated to a red fluorophore, CTB) and GABAergic neurons of the AON/APC using somatic viral infection. Likewise, dually-labelled cells were found scattered in the AOC, with a higher density in the AONp (Extended Data Fig. 1e).

SOM, PV and VIP characterize the vast majority of GABAergic neurons in the cortex and have been reported in largely non-overlapping populations in the AON[56] and APC[57]. To characterize the neurochemical nature of the OB-projecting GABAergic neurons, we first injected an AAV-Flex-ChR2-

TdTomato in the AON/APC of SOM-Cre, VIP-Cre or PV-Cre mice. Substantial axonal innervation in the OB was observed in SOM-Cre mice, while very sparse fibers were detected in PV-Cre and VIP-Cre mice (**Fig. 2d**). To assess the source of OB-projecting GABAergic neurons, we performed retrograde labeling in these transgenic mouse lines (HSV-Flex-GCaMP6f in the OB). Consistent with anterograde tracing, the highest density of retrogradely-labeled cells was found in SOM-Cre mice compared to VIP-Cre and PV-Cre mice (**Fig. 2d**). Densities of retrogradely-labelled cells were comparable between SOM-Cre and VGAT-Cre mice in the APC (cell density/mm^2 in VGAT-Cre, 6.0 ± 1.0; in SOM-Cre, 5.7 ± 0.3) and in the core of the AON (AONd: VGAT-Cre, 1.8 ± 0.8; SOM-Cre, 2.0 ± 0.5; AONl: VGAT-Cre, 4.6 ± 1.8; SOM-Cre, 2.9 ± 0.6; AONm: VGAT-Cre, 10.9 ± 1.9; SOM-Cre, 7.2 ± 1.0; see **Fig. 2c,e**). In contrast, the density of retrogradely-labeled cells was substantially lower in SOM-Cre compared to VGAT-Cre mice in the AONv (VGAT-Cre, 37.5 ± 6.4; SOM-Cre, 9.7 ± 0.2) and AONp (VGAT-Cre, 183.8 ± 15.4; SOM-Cre, 16.5 ± 0.6; **Fig. 2c,e**). We further characterized OB-projecting GABAergic neurons of the AON/APC using immunostaining. OB-projecting GABAergic neurons were identified by an HSV-Flex-GCaMP6f injection in the OB of VGAT-Cre mice. We confirmed the preferential expression of SOM in the GABAergic OB-projecting neurons of the APC (38.2% of all retrogradely-labeled neurons) and in the core of the AON (37.9 %), but not in the AONp (6.7%; **Fig. 2f,g**). Calbindin, however, was expressed in lower proportions but was more homogenous across the different regions of the AOC and was the main marker co-localizing with GABAergic OB-projecting cells in the AONp (15.6%; **Fig. 2f**; Extended Data Fig. 1g). VIP, PV or Calretinin were virtually not expressed in GABAergic feedback neurons. Altogether, these anatomical results show that, in parallel to the establish glutamatergic feedback, the AOC also sends GABAergic feedback to the OB. Inhibitory projection neurons were scatter in the AOC, with a substantial cluster in the AONp.

Cortical GABAergic projections target both OB principal cells and interneurons.

To identify the targets of cortical GABAergic projections, we first labeled putative pre- and post-synaptic components of the AOC-to-OB GABAergic synapses. Putative presynaptic elements were labeled using a Cre-dependent AAV expressing mRuby fused to the synaptic vesicle protein synaptophysin alongside GFP

in the axon shaft (Extended Data Fig. 2a). Putative postsynaptic elements were labeled using an immunostaining for the GABAergic receptor scaffolding protein gephyrin (Extended Data Fig. 2b). Apposition of synaptophysin and gephyrin was found directly on cell somas and presumed dendrites in the GCL, IPL, MCL and in the internal part of the GL. High densities of appositions were also found in the GCL (presumably on granule cell basal dendrites, GC) and EPL (presumably MC, TC and/or GC dendrites; Extended Data Fig. 2b). To functionally identify the targets of the cortical GABAergic inputs, we next employed an optogenetic-based circuit mapping approach. Channelrhodopsin-2 (ChR2) was expressed selectively in the GABAergic cells of the AON/APC and whole-cell recordings were obtained in acute OB slices (**Fig. 3a**). The light-evoked synaptic responses reflected direct GABAergic synaptic transmission as they were resistant to bath application of AMPA receptor antagonists (NBQX, 10 µM), but completely abolished by $GABA_A$ receptor antagonists (gabazine SR95531, 10 µM) (**Fig. 3b**). In deeper layers of the OB (GCL and IPL), evoked inhibitory postsynaptic currents (IPSCs) were detected in roughly half of the GCs (21/49) and in most of the deep short-axon cells recorded (dSACs, 9/12). In the MCL, half of the MCs (11/24) received direct inhibitory inputs. In superficial layers (EPL and GL), half of the eTCs (9/16) received direct inhibitory inputs, while PGs or sSACs did not (0/35 and 0/10 respectively). Light-evoked IPSCs displayed fast latencies (**Fig. 3c**) and kinetics (Extended Data **Table 1**). Inhibitory inputs were significantly greater in dSACs compared to any other cell type (**Fig. 3d**), in concert with previous observations with glutamatergic feedback[35,36]. Thus, cortical GABAergic feedback is directly and functionally connected with a diversity of neurons in the OB, regardless of whether they are excitatory or inhibitory, locally or distally projecting.

Optogenetic activation of cortical GABAergic inputs inhibits OB interneurons.

To assess the functional impact of the cortical GABAergic feedback on its main target layer (GCL), we employed fiber photometry in awake freely moving mice. The volume fluorescence of GCaMP6f-expressing GCL GABAergic neurons was continuously recorded in freely moving animals using an optic

fiber implanted above the injection site in the ventral OB (**Fig. 4a**). To specifically investigate the impact of the AOC GABAergic projections to the OB, we directly light-stimulated the axons in the OB (**Fig. 4a**). Using the red-shifted opsin ChRimson, we could independently control GABAergic axons and avoid cross-excitation of GCaMP6f[39,58]. Indeed, ChRimson light stimulation at 10 Hz, 33 Hz or with a continuous light step (CL) produced a global reduction of spontaneous activity in GCL GABAergic neurons while red light stimulation *per se* did not alter spontaneous activity in control animals (expressing GCaMP6f in the GCL, but not ChRimson in GABAergic feedback; **Fig. 4b**). The magnitude of the reduction of spontaneous activity was correlated with the light stimulation strength (**Fig. 4b**). This feature was still observed 1 s after light stimulation offset (**Fig. 4b**). In contrast to OB axon terminal stimulation, stimulation of GABAergic cell somas in the AON caused a variable and transient inhibition followed by rebound excitation, resulting in a global non-significant change of fluorescence (Extended Data Fig. 3b). This effect was likely produced by a general silencing of the AOC network and stresses the importance of direct axon stimulation for probing the functional impact of cortical GABAergic projections on the OB.

We next investigated the impact of GABAergic feedback stimulation on odor-evoked activity in the GCL. Odor stimulation induced a strong population response in GCL neurons[59] (**Fig. 4c,d**). To analyze the impact of ChRimson stimulation on odor-evoked activity, we quantified the net decrease in Ca^{2+} activity relative to the period before light stimulation, within the same odor response (**Fig. 4c**). When compared with odor response dynamics without light stimulation ("odor only"), ChRimson effectively dampened odor responses with 33 Hz and CL, but not 10 Hz, stimulation patterns (**Fig. 4d,e** and Extended Data Fig. 4c). 33 Hz and CL light inhibition of odor responses outlasted the light stimulation period (**Fig. 4d**). Increasing stimulation strength induced increasingly strong inhibition of odor-evoked responses during light stimulation (**Fig. 4e**). After light stimulation offset, CL caused a sustained inhibition that was stronger than with any other light stimulation pattern (**Fig. 4e**). Thus, cortical GABAergic axon stimulation efficiently drove inhibition of both spontaneous and odor-evoked activity in GCL GABAergic neurons, and the magnitude of this inhibition scaled with the stimulation strength of GABAergic axons.

Activation of cortical GABAergic inputs enhances the distance in TC population odor responses

To assess the impact of cortical GABAergic feedback activation on OB output neurons, we next performed awake two-photon Ca^{2+} recordings of MCs and TCs. Since our GCL photometry recordings showed that 33 Hz and CL stimulation induced greater responses, we employed the opsin ChIEF to yield more efficient and naturalistic drive of GABAergic axons[60]. The axon terminals were light-stimulated through the microscope's objective, while the photomultiplier tube (PMT) shutter was closed and reopened 50 ms before and after light onset and offset (**Fig 5a,c**). Due to the slow kinetics of GCaMP6s, we could capture Ca^{2+} events following the light offset and reopening of the shutter (**Fig. 5c,d**). MCs and TCs were identified based on the recording depth, the cytoarchitecture of each OB layer and the cell morphology and size[61–63] (**Fig. 5c**).

Light stimulation of cortical GABAergic axons induced a significant reduction of spontaneous activity in the large majority of the MCs and TCs (**Fig. 5d**; Extended Data Fig. 4a,b). In MCs, CL stimulation significantly reduced activity in a larger fraction of cells compared to 33 Hz stimulation, and inhibitory response magnitudes were larger (Extended Data Fig. 4a,b). These differences were not observed in TCs. This result was not an artifact of closing and reopening the PMT shutter. Indeed, in control trials, the number of cells exhibiting a significant change in activity was at statistical chance level, and the change in activity was significantly smaller, by an order of magnitude, than for light-stimulation trials ("shutter control": trials with shutter closing, but no light presented, **Fig. 5d;** Extended Data Fig. 4a,b). We additionally controlled for an effect of blue light illumination *per se* in control animals who did not express ChIEF. A small, yet above chance proportion of MCs and TCs showed significant reduction of activity, consistent with previous reports[64] (Extended Data Fig. 4b). However, the magnitude of the light-induced inhibitory responses was 10-fold bigger in ChIEF-expressing animals compared to control without ChIEF and therefore cannot significantly contribute to the reported effect (**Fig. 5d**).

GABAergic feedback inputs reduced spontaneous activity in the OB, but how does it influence incoming sensory feedforward information? Odor stimulation induced both inhibitory and excitatory

responses in MCs and TCs, but with different relative proportions, as previously reported[63,65,66] (**Fig. 5e**). In odor-responsive cells, stimulation of GABAergic cortical axons induced a reduction of excitatory odor responses and a greater inhibition of inhibitory odor responses. This was true across both cell types and light stimulation patterns. The magnitude of the light-evoked inhibition and the odor responses were not correlated, resulting in linear subtraction of the odor-evoked activity (**Fig. 5f**). Surprisingly, the magnitude of the light-evoked inhibition on spontaneous and odor-evoked activity was weakly correlated, indicating possible non-linear interactions between top-down GABAergic and bottom-up sensory inputs (Extended Data Fig. 4c).

To evaluate the effect of cortical GABAergic axon stimulation on the separation of odor representation in MC and TC populations, we calculated the Euclidean distance between population responses to either different ("Between odors") or the same odor (Within odor"; **Fig 5g**). Consistent with a linear subtraction of the odor responses in MCs and TCs, light did not significantly alter the pairwise distance between population responses to a given odor ("Within odor" design; **Fig 5g**). In contrast, in the "between odors" design, light stimulation increased the distance in population odor representation of TCs, but not MCs (**Fig 5g**). This suggests that stimulation of GABAergic axons increases the difference between responses to different odors, specifically in TCs.

Another recipient of GABAergic projections in the OB is the internal part of the GL. We thus targeted our recordings to juxtaglomerular cells (JG cells, at the transition between the GL and EPL). Similar to the MCs and TCs, CL stimulation of cortical GABAergic axons inhibited spontaneous activity of JG cells (Extended Data Fig. 4d). Odor stimulation drove mainly excitatory responses in JG cells, as reported previously[67] (Extended Data Fig. 4e). In the odor-responsive population, light stimulation of cortical GABAergic axons induced a linear reduction of the odor-evoked activity (Extended Data Fig. 4g). As seen in MCs and TCs, inhibition of spontaneous and odor-evoked activities was only weakly correlated (Extended Data Fig. 4g).

Cortical GABAergic inhibition to OB output neurons scales with the frequency of stimulation

Cortical glutamatergic feedback projections cause robust disynaptic inhibition onto MCs and TCs[35,36,39]. To qualitatively compare disynaptic and direct forms of cortically-driven inhibition, we employed a fiber photometry approach (Extended Data Fig. 5a,b). ChRimson stimulation of either cortical GABAergic axons or APC cortical glutamatergic neurons induced different frequency-dependent responses on MC/TC spontaneous activity (Extended Data Fig. 5c). Increasing stimulation strength of cortical GABAergic axons produced increasing inhibition of MC/TC activity. In contrast, disynaptic inhibition driven by APC cortical glutamatergic neurons stimulation peaked at 33Hz and decreased with higher frequencies (Extended Data Fig. 5d). Therefore, direct cortical inhibitory feedback is able to drive increasing inhibition in OB output cells with high-frequency stimulation, while the disynaptic cortical inhibition relayed by local GABAergic neurons works best at intermediate frequency.

Cortical GABAergic inputs entrain beta oscillations in the OB network

Oscillatory activities are prominent in the sensory systems where they participate in network synchronization and sensory perception[68,69]. In the OB, oscillations can be subdivided into different frequency bands reflecting different network interactions. Theta oscillations (1-12 Hz) largely reflect the sniffing modulation of olfactory sensory inputs while gamma oscillations (40-100 Hz) are locally generated by the OB network, through the reciprocal interaction between MCs and GCs[68]. Beta oscillations (15-40 Hz), however, require bidirectional connectivity between OB and olfactory cortex[42]. To explore the impact of cortical GABAergic projections on OB oscillations, we coupled optogenetic stimulation of cortical GABAergic axons with local field potential (LFP) recordings in the OB of awake VGAT-Cre mice (**Fig. 6a**). Theta, beta and gamma stimulation patterns (10, 33 or 66 Hz) were utilized to decipher the frequency at which GABAergic feedback impacts OB oscillations. 33 Hz light stimulation increased the power of spontaneous oscillation specifically in the beta band, while stimulation at 10 or 66 Hz had no significant effect (**Fig. 6b,c**). Thus, activation of cortical GABAergic feedback inputs, in the beta band, entrains OB oscillations in the same regime, which thus may enhance the coherence between the cortex and OB.

Silencing cortical GABAergic outputs to the OB affects fine odor discrimination

To test the contribution of cortical GABAergic feedback on olfactory behavior, we took a pharmacogenetics approach using designer receptors exclusively activated by designer drugs (DREADD). Inhibitory DREADD (hM4Di) was expressed in GABAergic AON/APC neurons and their axon terminals in the OB were selectively silenced by locally infusing the ligand, clozapine-*N*-oxide (CNO; **Fig. 7a**). In a go/no-go task, the mice detection and discrimination thresholds were evaluated using carvone and limonene enantiomers (**Fig. 7b**). Detection threshold was assessed by diluting each day by a factor of 10 the two enantiomers to detect (from 1% to 0.0001% dilution). Discrimination threshold was assessed by presenting binary mixtures of the enantiomers, with a progressive and symmetric increase of the proportion of one into the other each day (from pure enantiomers discrimination, i.e. 100:0 vs 0:100, to discrimination of mixtures with 55:45 vs. 45:55 enantiomer ratios). Local CNO injection had no effect on the detection of carvone or limonene enantiomers, even at very low odor concentration (**Fig. 7c**). In contrast, CNO-mediated inhibition of GABAergic feedback impaired the discrimination of very similar binary mixtures of enantiomers. Indeed, a significant decrease in discrimination was observed for limonene enantiomers. For carvone enantiomers, a similar reduction in performance was observed, although not statistically significant (**Fig. 7c**). When discrimination performances were analyzed collectively for both pairs of enantiomers, CNO significantly reduced fine discrimination performances over the last three blocks in h4MDi-expressing mice (discrimination of carvone and limonene enantiomer mixtures at 55:45 vs 55:45 analyzed together; **Fig. 7c**). No significant difference in odor sampling time was observed (evaluated for correct rewarded trials in sessions with performance greater than or equal to the 85% criterion; Extended Data Fig. 6). Altogether, the behavior data suggests that silencing cortical GABAergic axon outputs to the OB impairs fine odor discrimination.

Discussion

This study reveals the presence of GABAergic feedback projections from the primary olfactory cortex to the OB. We showed that cortical GABAergic feedback to the OB forms functional synapses with both GCL interneurons and principal output neurons. In vivo, this feedback had a net inhibitory effect in all cell types tested. In OB output neurons and local interneurons, the magnitude of cortical inhibition increased with the degree of light stimulation. Cortical inhibition and sensory response magnitudes were not correlated, resulting in a linear subtraction of MCs and TCs odor-evoked activity as well as a reduction of odor response similarity in specifically in TCs. GABAergic feedback stimulation was also able to entrain OB network oscillations specifically in the cortex-OB communication regime (beta band, 20-40 Hz). Silencing of cortico-bulbar inhibitory axons altered performances during a fine odor discrimination task. Lastly, we reported an analogous inhibitory cortico-thalamic projection in the somatosensory system, indicating that cortical GABAergic feedback represents a new canonical circuit motif in sensory systems.

GABAergic OB-projecting cells are diverse in the olfactory cortex. We identified a sparse population of GABAergic projections neurons scattered in the main part of the AON and in the APC, preferentially expressing SOM. We additionally identified a dense cluster of GABAergic projection neurons in the AONp (at the border between the AONv, APC and OT), which do not preferentially express SOM. Non-specific retrograde labeling studies had already identified a cluster of OB-projecting cells in the AONp in hamsters[31,70], rats[29,71] and mice[34,49,72,73], yet their neurochemical content had not been specified. As a first step to decipher the functions of cortical GABAergic feedback in sensory systems, here we investigated these inputs as a homogeneous functional unit. However, diversity in the sources of GABAergic projection neurons in the AON could result in diverse targeting across layers and cells in the OB, and could be associated with different functions (similarly to the glutamatergic feedback). Nevertheless, silencing cortical GABAergic feedback axons disrupted fine sensory discrimination of similar odor mixtures, consistent with a role of corticofugal projections in switching the balance between sensory

detection and discrimination[74]. Stimulating GABAergic feedback reduced MC and TC odor responses, and stimulation in the beta band specifically strengthened OB beta oscillations. Beta oscillations have been shown to emerge during odor discrimination learning and require intact communication between the OB and the olfactory cortex[68,75]. Moreover, precise spike timing of MCs and TCs relative to OB oscillations is critical for coding of odor intensity[76–79], odor identity[80] and increases during olfactory learning[81]. Thus, altering the tightly regulated spike-field coherence could be a mechanism through which cortical GABAergic feedback could directly shape sensory perception (see below for circuit considerations). Additionally, we reported that GABAergic feedback stimulation had a net suppressive effect on MCs and TCs. Manipulating the inhibitory tone onto MCs and TCs has been shown to influence output cell correlations and discrimination performance[82]. Here, we showed that cortical GABAergic inputs stimulation enhanced the differences in population responses to two different odors, suggesting a neuronal mechanism for the role of cortical GABAergic feedback in shaping sensory perception. Interestingly, pattern decorrelation in odor response took place in the TC, but not MC population. Given that TCs preferentially innervate the anterior part of the olfactory cortex[83], and specifically the AON ventroposterioralis[84] – the major source of cortico-bulbar GABAergic projections, this result supports the notion of preferred interaction between looped circuit elements, as suggested in the neocortex[85,86]. Altogether, decreasing the activity of output neurons, reducing the similarity between sensory inputs and controlling the proper establishment of sensory-evoked network oscillations are three mechanism through which GABAergic feedback can directly shape sensory perception.

The two forms of extrinsic inhibition to the OB, cortical and from the basal forebrain, exhibited different innervation patterns across OB layers. Both innervated the MCL, but while basal forebrain GABAergic axons extensively innervated the GL and the external part of the EPL, cortical axons did not. In the GL, this resulted in differential targeting of MC and TC presynaptic partners[53–55,87,88]. In the EPL, it may result in a differential targeting of MC and TC functional subcellular domains (apical dendrites, proximal or distal lateral dendrites). This differential innervation by both direct GABAergic feedback projections

could be the cause of their differential impact on MCs and TCs. While spontaneous activity was inhibited by both projections, odor-evoked activity was enhanced upon basal forebrain GABAergic input stimulation and suppressed upon cortical GABAergic input stimulation[88].

Direct GABAergic cortical inhibition also differs from the disynaptic cortical inhibition pathway where cortical glutamatergic inputs are relayed by local GABAergic neurons – where it produces excitation followed by inhibition. The temporal properties of the direct excitation are under tight control of disynaptic inhibition[39]. In olfaction, cortical glutamatergic feedback is relayed by local GABAergic neurons[35,36] in the OB, while in the neocortex cortical glutamatergic feedback is relayed by GABAergic neurons in reticular thalamic nucleus[89]. In the OB, stimulating cortical glutamatergic projections yields optimal inhibition of MCs and TCs in the beta range (20-40Hz) and decreases with faster stimulation regimes[39]. Similar frequency-dependent activity also takes place in lower-order thalamic nuclei: low-frequency cortico-thalamic axon stimulation suppresses thalamic activity while high-frequency stimulation enhances it[89,90]. In both systems, GABAergic relay neurons seem to implement band-pass filtering of the cortical glutamatergic drive. In contrast, the strength of the inhibition in MCs and TCs scaled with the strength of cortical GABAergic axons stimulation, even at high frequency regimes. Similarly, in the thalamus, direct extrathalamic GABAergic innervation from subcortical nuclei display a high fidelity to fast stimulation regimes[91]. Thus, the direct cortical inhibition of lower-order somatosensory thalamic nuclei reported in this study might provide dynamic control of thalamic excitability, even at high-frequency. Additionally, cortical GABAergic projections can have a modulatory effect on the excitation/inhibition dynamics of postsynaptic neurons by activating presynaptic $GABA_B$ receptors present at specific glutamatergic axon terminals[39]. Thus, cortical GABAergic feedback is ideally positioned to relax the excitation window for OB or thalamic output neurons in response to cortical glutamatergic activation[35,39,45].

Our study describes the functional impact of the GABAergic cortical feedback to the OB and set the basis for deciphering the function of a novel corticofugal pathway: direct GABAergic cortico-subcortical

projection from S1 to the somatosensory thalamic nuclei. Cortico-subcortical GABAergic feedback is therefore a shared circuit motif across different sensory modalities and across the paleocortex and neocortex. In the brain, looped interactions are therefore not only excitatory, but also integrate an inhibitory component. What is the function of inhibitory projections in looped computations? In the hippocampus-entorhinal cortex, they synchronize distant structures and gate spike timing of CA1 pyramidal cells[11,92]. In a sensory system, we show here that inhibitory projections are involved in oscillatory activities, gain control, increasing pattern decorrelation and fine sensory discrimination. Results from this study will pave the way to further deciphering the impact of cortical gating of subcortical sensory processing.

Material and Methods

Animals.

Adult male and female VGAT-Cre (heterozygotes, Slc32a1$^{tm(cre)Lowl}$, MGI ID: 5141270), SOM-Cre (Ssttm2.1(cre)Zjh, MGI ID: 4838416), VIP-Cre (Viptm1(cre)Zjh, MGI ID: 4431361) and PV-Cre (Pvalbtm1(cre)Arbr, MGI ID: 3590684) were used in this study. This work was performed in compliance with the French application of the European Communities Council Directive of 22 September 2010 (2010/63/EEC) and approved by the local ethics committee (CETEA 89, project #01126.02, #2013-0086 and #DAP20025).

Stereotaxic injections.

Adeno-associated viruses (AAV) were generated by the Penn Vector Core, University of North Carolina Vector core, Addgene or produced by the Institut National de la Santé et de la Recherche Médicale (INSERM, UMR 1089, www.atlantic-gene-therapies.fr). Herpes simplex viruses (HSV) were produced by the MIT gene transfer core. CTB conjugated to Alexa Fluor 555 (C34776) was obtained from Molecular probes. For viral injections, mice were deeply anesthetized using ketamine and xylazine mixture (150 mg/kg Imalgene and 5mg/kg Rompun, respectively; i.p.) and placed in a stereotaxic apparatus. A small craniotomy was performed, and a viral/CTB solution was injected into the brain through a glass micropipette attached to a Nanoinjector system (Nanoject II, Drummond). The coordinates and volumes used for injections were as follows: AON: 2.3 mm anterior and 1.1 mm lateral from Bregma, 3.3 and 3.5 mm deep from the brain surface, 100 nL/site; APC: 1.9 mm anterior and 2.25 lateral from Bregma, and 3.8 and 4.2 mm deep from the brain surface, 150-200 nL/site; NDB/MCPO: 0.1 mm anterior and 1.5 mm lateral from bregma, 5.5 deep from brain surface, 100nl/site; Somatosensory cortex S1, barrel field (BFC): 1 mm anterior and 3 mm lateral from Bregma, 1.2 and 1.5 mm deep from brain surface, 200nl/site. OB: 1mm anterior and 1mm lateral from junction of inferior cerebral vein and superior sagittal sinus, 1, 1.5 and 2mm

deep from the brain surface, 100 nL/site. OB Lateral GL: 1mm anterior and 2mm lateral from junction of inferior cerebral vein and superior sagittal sinus, 1.5 from brain surface, 50nl/site. Larger volumes were used for dual-labeling of OB-projecting GABAergic neurons (Extended Data Fig. 1): 150nL/site in the AON and 300nL/site in the APC.

Virus	**Injection site**	**Titer**	**Source**
AAV2/5-EF1a-DIO-hChR2(H134R)-eYFP	AON/APC (Fig. 1 and Fig. 3)	1.8x 10^{13}	Plasmid: Addgene#20298 Production: INSERM U1089 Vector Core
AAV2/9-hSyn-DIO-ChrimsonR-TdTomato	NDB/MCPO, BFC (Fig. 1) AON/APC (Extended Data Fig. 1, Fig. 4, Extended Data Fig. 3, Extended Data Fig. 5)	4.5x 10^{12}	UNC Vector Core
AAV2/9-hSyn-ChrimsonR-TdTomato	APC (Extended Data Fig. 5)	5 x 10^{12}	Penn Vector Core
HSV-hEF1-Flex-GCaMP6f (LT)	OB (Extended Data Fig. 1)	1x10^{8}	MIT gene transfer core
AAV2/9-CaMKIIa-hChR2(H134R)-eYFP	AON/APC (Extended Data Fig. 1) BFC (Fig. 1)	2 x 10^{13}	Plasmid: Addgene#26969 Production: INSERM U1089 Vector Core
AAV2/1-hSyn-DIO-GCaMP6f	OB (Fig. 4, Extended Data Fig. 3)	1.7 x 10^{13}	Penn Vector Core
AAV2/9-DIO-GFP-IRES-Synaptophysin-mRuby	AON/APC (Extended Data Fig. 2)	5.7 x 10^{12}	Plasmid: Addgene#71760 Production: INSERM U1089 Vector Core

AAV2/1-hSyn-GCaMP6s	OB (Fig. 5, Extended Data Fig. 4)	2.1 x 10^{13}	Penn Vector Core
AAV2/1-hSyn-GCaMP6f	OB lateral GL (Extended Data Fig. 5)	1.2 x 10^{13}	Penn Vector Core
AAV2/5-CAG-DIO-ChIEF-TdTomato	AON/APC (Fig. 5, Fig. 6, Extended Data Fig. 4)	5.5x10^{12}	Plasmid: Addgene#30541 Production: INSERM U1089 Vector Core
AAV2/5-hSyn-DIO-hM4Di-mCherry	AON/APC (Fig. 7)	6.5x10^{12}	UNC Vector Core

Histology.

Tissue preparation: Animals were intracardially perfused (4% paraformaldehyde (PFA) in 0.1M phosphate buffer) and the brains were removed and post-fixed in the same fixative overnight. Brain sections were then cut with a freezing microtome (Leica). For post-hoc analyses of recording sites and viral expression, 100 µm-thick sections were sliced. OB sections were inspected to check for proper axonal expression, absence of virus diffusion into the OB, and for the absence of significant somatic labeling in the OB. 50 µm-thick sections were used for anatomical analyzes. Animals in which post-hoc histological examination showed that viral injection were not in the correct location were excluded from analysis.

Immunohistochemistry*:* Primary and secondary antibodies used in this study are summarized in Table 2. Immunochemistry labeling was performed as follows: slices were rinsed, permeabilized and blocked in 10% Normal Goat Serum and PBS containing 0.25% Triton-X100 (PBST) for 2h. Primary antibodies were then incubated for up to 48h at 4°C in PBST containing 1% serum and 0.01% azide, washed three times and secondary antibodies were finally added for 2h in PBST containing 2% serum. Slices were then rinsed

and counterstained with DAPI, mounted and imaged with a confocal microscope (LSM 700, Zeiss) or epifluorescence microscope (Axiovert 200, Zeiss) equipped with an Apotome system (Zeiss).

Cell counting of retrogradely-labeled cells*:* One out of every three 50 µm-thick coronal slices were serially collected from OB to amygdala (-2 from bregma) and analyzed for cell soma quantification. To evaluate cell density, immunopositive cell soma were manually counted and brain regions were manually delineated using morphological parameters, DAPI staining, immunohistochemistry labeling and the Allen Brain reference Atlas. Values for each subregion are averaged across sections for each mouse. The number of labelled cells per regions relative to the total number of cells counted per animal were also calculated and reported as percentage.

Density of fluorescent axons in the dorsal OB region of coronal slices was determined using the ImageJ plugin "plot profile". Measurements were performed in matching slices and averaged across section per animal.

Primary Antibodies			
Raised against	**Host species**	**Dilution**	**Source**
Calbindin D-28k	Mouse (monoclonal)	1:2,000	Swant 300
Calretinin	Rabbit (polyclonal)	1:2,000	Swant 7697
ChAT	Goat (polyclonal)	1:200	Millipore AB144P
GAD67	Mouse (monoclonal)	1:1,000	Merck Millipore MAB5406
GAD 65/67	Rabbit (polyclonal)	1:1,000	Sigma G5163

GFP	Chicken (polyclonal)	1:4,000	Abcam ab13970
Parvalbumin	Rabbit (polyclonal)	1:2,000	Swant PV27
Somatostatin	Goat (polyclonal)	1:500	Santa Cruz D20
Vasoactive intestinal peptide	Rabbit (polyclonal)	1:1,000	Immunostar 20077
RFP	Rabbit (polyclonal)	1:4,000	Rockland Inc. 600-401-379

Secondary antibodies			
Raised against	**Host species**	**Dilution**	**Source**
Alexa 488			
anti-Chicken	Goat	1:1,000	Molecular Probes A-11039
anti-Rabbit	Goat	1:1,000	Molecular Probes A-11034
anti-Rabbit	Donkey	1:500	Jackson 711-546-152
anti-Goat	Donkey	1:500	Jackson 705-546-147
Alexa 568			
anti-Rabbit	Goat	1:1,000	Molecular Probes A-11036
Cy5-conjugated			
anti-Mouse	Goat	1:1,000	Jackson 115-175-166

anti-Rabbit	Goat	1:1,000	Jackson 111-175-144

Electrophysiology.

Mice were deeply anesthetized with intraperitoneal injection of ketamine (100 mg/kg) and xylazine (10 mg/kg) and swiftly decapitated. The OB and frontal cortices were rapidly dissected and placed in icecold artificial cerebrospinal fluid (ACSF) containing 124 mM NaCl, 3 mM KCl, 1.3 mM MgSO4, 26 mM NaHCO3, 1.25 mM NaHPO4, 20 mM glucose, 2 mM CaCl [~310 mOsm, pH 7.3 when bubbled with a mixture of 95% O2 and 5% (vol/vol) CO2; all chemicals from Sigma-Aldrich]. Horizontal slices (300-µm thick) of the OB were placed in bubbling ACSF in a warming bath at 35 °C for 30 min and then at room temperature (i.e., 22 ± 1 °C). For whole-cell recordings, individual slices were placed in a chamber mounted on a Zeiss Axioskop upright microscope, and continuously perfused (1.5 mL/min) with 30°C ACSF (Warner Instrument inline heater). Slices were visualized using a 40× water immersion objective.

We obtained whole-cell patch-clamp recordings from visually targeted GCs, MCs, dSAC, PGc, sSAC, ETC. Neuron types were identified by their laminar location, morphology, and intrinsic properties. For glomerular layer recordings, juxtaglomerular cells were filled with fluorescent dye (Alexa 488, 40 µM) and classified based on morphological and electrophysiological criteria[93,94]. ET cells were identified as having large (~20 µm) somata, a single dendrite and tuft ramifying within one glomerulus, an axon extending into the EPL and a relatively low input resistance (197 ± 36 MΩ, n = 10). PG cells were distinguished by their small somata (~10 µm diameter) and high input resistance (~1 GΩ). sSACs were distinguished by their unique dendritic arbors that are exclusively periglomerular, span multiple glomeruli, lack tufts, and are poorly branched[36].

Patch pipettes, pulled from borosilicate glass (OD 1.5 mm, ID 0,86 mm; Sutter instrument; P-87 Flaming/Brown micropipette puller, Sutter Instruments), had resistances of 6–10 MΩ for GCs and PGCs recordings and of 3-5 MΩ and were filled with a cesium gluconate-based solution: 126 mM Cs-gluconate,

6 mM CsCl, 2 mM NaCl, 10 mM Na-Hepes, 10 mM D-glucose, 0.2 mM Cs-EGTA, 0.3 mM GTP, 4 mM Mg-ATP, 280–290 mOsm, pH 7.3). Membrane potentials indicated in the text are corrected for a measured liquid junction potential of +10 mV. Recordings were obtained via an Axon Multiclamp 700B. Synaptic events were elicited by photo-activation of $ChR2^{+}$ axon terminals stimulation using a 470-nm LED (Xcite by Lumen Dynamics) illuminating the sample trough the objective. Inhibitory postsynaptic currents (IPSCs) were recorded at Vc = 0 mV. Rise times were measured between 10% and 90% of peak amplitude. For IPSCs, decay time constants were derived by fitting the sum of two exponentials: $F(t) = a \times \exp(-t/t\ fast) + b \times \exp(-t/t\ slow)$, where a and b are the peak amplitude of fast and slow components, respectively, and t fast and t slow are the respective decay time constants. Data were acquired using Elphy software (Gerard Sadoc, Centre National de la Recherche Scientifique; Gif-sur-Yvette, France) and analyzed with Elphy and IgorPro (Neuromatic by Jason Rothman, www.neuromatic. thinkrandom.com).

Calcium imaging using fiber photometry.

We used a fiber photometry system adapted from Gunaydin et al., 2014[95]. Immediately following GCaMP6f virus injection in the OB, AON or APC, optical fibers (multimode, 430 µm in diameter, NA 0.5, LC zirconia ferrule) were bilaterally implanted close to the virus injection site, in the ventral part of the OB for GCL recording (1mm anterior and 1mm lateral from junction of inferior cerebral vein and superior sagittal sinus, 2mm deep from the brain surface, for Fig. 4 and Extended Data Fig. 3) and in the lateral part for MC/TC recordings (1mm anterior and 1.5mm lateral from junction of inferior cerebral vein and superior sagittal sinus, 1.5mm deep from the brain surface, for Extended Data Fig. 5) and then secured to the skull with a liquid bonding resin (Superbond, Sun Medical) and dental acrylic (Unifast). Three weeks post-injection, GCaMP6f was continuously excited using a 473 nm DPSS laser (output fiber intensity: < 0.1 mW; Crystal Lasers) reflected on a dichroic mirror (452-490 nm/505-800 nm) and collimated into a 400 µm multimode optical fiber (NA, 0.48) with a convergent lens (f = 30 mm). The emitted fluorescence was collected in the same fiber and transmitted by the dichroic mirror, filtered (525 ± 19 nm) and focused on

a NewFocus 2151-femtowatt photoreceptor (Newport; DC mode). Reflected blue light along the light path was also measured with another amplified photodetector (PDA36A, Thorlabs) for monitoring light excitation and fiber coupling. Red light (589 nm, 10 mW, pulse duration: 10-15ms) was collimated in the recording optic fiber to selectively activate cortical ChRimsonR-expressing GABAergic axon terminals in the OB while GCaMP6f was independently excited with low blue light intensity (< 0.1 mW), thereby avoiding cross-excitation of Chrimson (as in Mazo et al., 2016[39]). Sessions with significant averaged changes in the reflected blue light (> 1% ΔF/F) were discarded from the analysis. Signals from both photodetectors were digitized by a digital-to-analog converter (DAC; Power 1401, CED) at 5 kHz and recorded using Spike2 software. For AON or APC stimulation using ChrimsonR, an optic fiber (multimode, 430µm diameter, NA 0.39, with LC zirconia ferrule) were bilaterally implanted above the AON (2.3 mm anterior and 1.1 mm lateral from Bregma, 3.3 deep from the brain surface ; Extended Data Fig. 3) or APC (1.9 mm anterior and 2.25 lateral from Bregma, 3.8 deep from the brain surface; Extended Data Fig. 5) and connected to a DPSS laser (589 nm, CNI Lasers; 10 mW output fiber intensity) via a custom-built fiber launcher.

Mice were placed in small, ventilated cage (~0.5L). Using a custom-built air-dilution olfactometer controlled by the CED card, pure monomolecular odorants were diluted in mineral oil and saturated odorized air was further mixed with the air stream (1/10 dilution) before being delivered into the ventilated cage (flow rate of 3L/min), thanks to solenoid pinch valves. Odors were presented for 5 s every 60 s and dynamics of odor presentation in the cage were constantly monitored using a mini photoionizer detector (miniPID, Aurora). Odors used were: Acetophenone 1%, Anisol 1%, Carvone+ 5%, Decanal 5%, Ethyl-butyrate 0.5%, Geraniol 5%, Heptanal 1% Hexanone 0.5%, 2-methyl-butyraldehyde 1%, Pentanol 1%, Valeraldehyde 0.2%, Methyl Salicylate 2%, 3-methyl-3-penten-2-one 1%. The 589 nm light stimulation was applied during 1 s, 3.5 s after odor onset when odor and light were simultaneously presented as well as 30s after odor presentation. Cycles of odor, light, and odor + light presentations were repeated 10 times for each condition. *S*ignals were smoothened (0.02 s window) and downsampled to 500 Hz. For each trial,

the signal was normalized to the baseline fluorescence of the trial using the ΔF/F ratio with F_0 being the average fluorescence 2 sec before the beginning of the trial. After completion of the recordings, mice were deeply anesthetized and transcardially perfused with 4% paraformaldehyde. OB and AOC were cut into 60µm-thick slices and observed with light and epifluorescence microscopes to evaluate the correct position of the optical fibers and the correct expression and diffusion of the virus. Animals in which post-hoc histological examination showed that viral injection or implanted optic fiber were not in the correct location were excluded from analysis. Selected sections were counterstained with DAPI and mounted for image acquisition (Axiovert 200 with Apotome system, Zeiss).

Calcium imaging using two-photon microscopy

Acquisition parameters and imaging: After viral injections, a cranial window (3.0x1.4 mm glass) was placed over both OB and a stainless-steel head bar (L-shaped) was cemented to the skull. Mice were then allowed to recover for a month. During this period, the animals were progressively habituated to the head fixed position while staying quiet in the 50-ml open-ended support tube. Calcium activity was imaged using a two-photon system (950 nm, Spectra Physics) with a Prairie Investigator microscope (Bruker) and equipped with GaAsP photomultiplier tubes (PMTs). Ca^{2+} transients were imaged using a 16X, 1.05 NA microscope objective (Nikon) with a 2X digital zoom. The field of view was 512x512 pixels (423.7x423.7µm), imaged at 15 Hz using a resonant galvanometer. Imaging planes (MCL, EPL or GL) were determined using anatomical landmarks and layers depth profiles as in [96]. Mean recording depth (relative to the GL) ± s.d: MCL, 201.8 ± 29.9µm; EPL, 60.1 ± 20.7µm.

Stimulation protocols: Trials consisted in 8s baseline, 2s stimulation (odor, light or odor+light) and 10s inter-trial interval. Trials were grouped in blocks of 20 trials. 2-3 blocks were acquired per stimulus type. Data was acquired from 6 OBs of 4 animals.

Light activation of GABAergic cortical axons. The LED illumination for full-field photo-activation feature of the Investigator series (Bruker) was used to photo-stimulate the GABAergic axons in the OB. Blue light was

directed to the field of view through the microscope objective. The PMT shutter remained closed during the photo-stimulation period and GCaMP6s fluorescence light was collected before and 50ms after the stimulation for allowing bidirectional realignment of the scanning. This time-window was evaluated using control trials were the light shutter closed but in the absence of photo-stimulation. GCaMP6s photo-bleaching using our ChIEF^{+} axon photo-activation paradigm was assessed by applying the same protocol to mice expressing GCaMP6s solely and was not minimal.

Odorant delivery. The odor pairs were a natural odor pair (curry powder *vs*. cinnamon) or a pair of pure monomolecular odorants (ethyl butyrate, valeraldehyde, isoamyl acetate, ethyl tiglate, hexanone or cineole, Sigma-Aldrich). Pure odorants were diluted 1:10 in 10mL mineral oil and natural odorants were presented in their native state. Saturated odor vapor was further diluted with humidified clean air (1:10) by means of computer-controlled solenoid pinch valves. Odor presentation was performed using a custom-built computer interface. Odor delivery dynamics were monitored and calibrated using a mini-PID (Aurora). Odors were delivered randomly within a block (10 trials of each odorant).

Odor and light stimulation. In "Odor + Light" trials, odorants and light were presented simultaneously utilizing the protocols mentioned above. After completion of the recordings, mice were transcardially perfused with 4% paraformaldehyde. OB and AOC were cut into 60µm-thick slices and observed with light and epifluorescence microscopes to evaluate the correct expression and diffusion of the virus. Selected sections were counterstained with DAPI and mounted for image acquisition (Axiovert 200 with Apotome system, Zeiss).

Image analysis:

Motion correction. A full field of view motion correction was performed using a custom-made program in MATLAB. A two-dimensional cross-correlation of every frame with the average projection of the entire image set was used to identify the out of frame z-movements (Pearson's r >0.65 in the 2D cross-correlation). For lateral motion correction, the established ImageJ plugin MoCo[97] was used. In brief, it uses a Fourier-transform to improve the efficacy for identifying translational motion.

Principal component analysis (PCA) assisted reconstruction. We employed PCA on the raw motion-corrected datasets, after concatenating all the trials for each experiment into a 3-dimensional matrix. It leads to the possibility to express the original data in a lower dimension, essentially capturing the largest variability in the dataset. Since the non-varying pixels and noise in the dataset do not have high variability across time, it gives us a reliable way of reconstructing the original image set from the most variable eigenvectors. The reconstruction was done by a linear combination of the PC scores and the PC coefficients for the first 10 PCs of the dataset.

Identification of regions-of-interest (ROIs). The PCA-reconstructed images were used for the identification of ROIs. ROIs were manually drawn on the cell bodies using ImageJ and were imported in MATLAB. In order to remove the contribution of neuropil and background fluctuation of each individual ROI from the extraction, we performed a second PCA inside the ROI encompassing all the image pixels. We took advantage of the orthogonality of PCA and determined the coordinates of each ROI using the first PC for reconstruction. The resulting reconstruction redefined the outer bounds of each ROI and increased the robustness for activity quantification. This process eliminated noisy signals and improved signal-to-noise ratio by 25% (Saha et al, in preparation). Mean size of ROIs ± s.d: MCs, 138.6 ± 50.8 μm^2; TCs, 138.7 ± 48.1 μm^2; JG cell, 90.6 ± 42.8 μm^2. For comparison, GC ROI size is 71.6 ± 32.0 μm^2 (Saha et al., in preparation).

Data analysis:

Z-score calculation. For each ROI, the pixel intensities were smoothed across 5 frames and *z-score* was calculated for each cell as follow:

$$z = \frac{\mu resp - \mu baseline}{\sqrt{\sigma resp^2/n - \sigma baseline^2/n}}$$

With μ and σ being the mean and standard deviation; resp, response (1 s after shutter reopening) and baseline is 1s before shutter closes. n is the number of trials. For comparison, we show in Extended Data Fig. 4 ΔF/F values, with F0 being the baseline determined for each trial.

Individual cell response to ChIEF light stimulation was considered significant if it passed a paired t-test based on single trials, with an alpha threshold of 0.01. Response and baseline values were the mean values 1s after and 1s before the shutter closed and reopened, respectively.

Light responsive cells were identified using a two-sided paired t-test on single trials, with an alpha threshold of 0.01. Response and baseline values were the mean values 1s after and 1s before the shutter closed and reopened, respectively.

Odor responsive cells were identified using a two-sided paired t-test on single trials, with an alpha threshold of 0.05.

Euclidean distance. For each recording session (7 for MCs, 9 for TCs), pair of population vectors were constructed from the averaged z-score responses to either the two odors presented on that day (Between odors design), or to the same odor (Within odor design). Only the cells responding to both odors (Between odors) or to the given odor (Within odor) were selected. Sessions were kept if a minimum number of 5 cells were responding to an odor. Pairwise Euclidean distance was calculated on the population vectors in the remaining sessions.

The Euclidean distance between two vectors *p* and *q* is given by the formula:

$$d(p,q) = \sqrt{(p-q)(p-q)'}$$

Olfactory Behavior

Two-guide cannulas (26-gauge, 7 mm long) were bilaterally implanted over the dorsal surface of the OB on the same day as viral injections 1mm anterior and 1mm lateral from junction of inferior cerebral vein and superior sagittal sinus. Guide cannulas were stabilized with a liquid bonding resin (Superbond, Sun Medical) and dental acrylic (Unifast) and a dummy cannula was positioned in the guide cannula to prevent blocking. Mice were habituated to be handled and maintained still while manipulating the dummy cannulas. On the day of the experiment dummies were retrieved, cannulas (8.5mm long, to inject at 1.5mm below the surface of the brain, 33-gauge and connected to a 10 µL Hamilton syringe) were placed for injections into the GCL. Dummies were put back in place a few minutes after the end of the injection.

Behavior experiments were conducted using a go/no-go operant conditioning scheme as previously described. 2 weeks after the surgery, aged-matched adult male VGAT-Cre mice (10-12 weeks old) were partially water-deprived (maintained at 80-85% of their baseline body weight) and trained in custom-built computer-controlled eight-channel air-dilution olfactometers (Alonso et al., 2012; for more details see www.olfacto-meter.com). Briefly, solenoid pinch valves controlled purified air streams, passing over the surface of mineral oil-diluted odorants. The odorized air was diluted 1:40 in odor-free air before its introduction into an odor sampling tube in the mouse operant chamber. Standard operant conditioning methods were used to train mice to insert their snouts into the odor sampling port for at least 1 s and to respond by licking the water delivery tube located at 5 cm left of the odor port to get a water reward (3 µl). An infrared detection system continuously monitored the presence of the animal in the odor port. After this training phase to learn the procedure (200 trials per day for 5 days), mice had to learn to lick in the presence of a positive odor stimulus S+ and to refrain from licking and retract their head from the sampling port in the presence of a negative odor stimulus S-. In each trial, a single stimulus was presented and S+ and S- trials were presented in a modified pseudo-random order. Inter-trial intervals were minimum 8s-long. Each mouse performed a maximum of 10 blocks (200 trials) per day. The percentage of correct responses was determined for each block of 20 trials. A score of 85% at the very least implied that mice had correctly learned to assign reward/non-reward values. Odor sampling time was the time between the opening of the final valve and head retraction out of the odor sampling port.

Initial odor-reward learning, without intrabulbar injection, was performed using Anisole (S+) and Heptanone (S-). All the mice learned the behavioral procedure and were able to discriminate the two odors (behavioral performance > 85%) within three days. Three additional days of training were performed to ensure performance stabilization. Then mice were first trained with limonene enantiomers [S+, (+)-limonene; S-, (-)-limonene] and then carvone enantiomers [S+, carvone-(+); S-, carvone-(-)]. Detection threshold was assessed by diluting each day by a factor of 10 the two enantiomers to detect (from 1% to 0.0001% dilution). Discrimination threshold was assessed by utilizing binary mixtures of the enantiomers,

with a progressive and symmetric increase of the proportion of one into the other each day (from pure enantiomers discrimination, i.e. 100:0 vs 0:100, to discrimination of mixtures with 55:45 vs. 45:55 enantiomer ratios). To induce pharmacogenetic silencing before each different olfactory task, mice underwent bilateral intrabulbar injection of CNO or vehicle (saline) through the guide cannula (CNO final concentration: 0.1 mg/mL, injection speed: 0.33µL/min for 3 min, 1µL total/bulb) and were left in their home cage for 15-20 min to allow CNO or vehicle (saline) diffusion within the OB, before being placed in the olfactometer. The control group was composed of mice expressing mCherry in cortical GABAergic axons without the h4MDi receptor injected with CNO (controlling for CNO side-effects, n=6) and mice expressing h4MDi in cortical GABAergic axons injected with saline (controlling for any non CNO-dependent side effect of expressing the exogenous h4MDi receptor, n=3). For CNO injections, experimenters were blind relative to the viral constructs expressed in individual mice. For behavior, animals which did not perform the 200 trials in the 60min time period following CNO injection were discarded from the analysis. After completion of the behavioral experiments, mice were transcardially perfused with 4% paraformaldehyde. OB and AOC were cut into 60µm-thick slices and observed with light and epifluorescence microscopes to evaluate the correct position of the injection cannula and the correct expression/diffusion of the virus. Animals in which post-hoc histological examination showed that transgene expression were not restricted to the AON were excluded from analysis. Selected sections were counterstained with DAPI and mounted for image acquisition (Axiovert 200 with Apotome system, Zeiss).

Statistical analysis

Sample sizes are indicated in the figure and/or in the legend of the corresponding figures. All statistics were performed using GraphPad Prism 8 or MATLAB. Data containing two experimental groups were analyzed using unpaired two-sided Student's t-test (parametric observations), unpaired two-sided Mann–Whitney test (non-parametric observations), one-way and two-way ANOVA tests followed by Tukey's post hoc analyses to account for multiple comparisons. Linear regression and slope comparison were analyzed using ANCOVA test. Data containing multiple paired measures (across time or stimulation frequency) were

analyzed using repeated-measures ANOVA test. The mean and s.e.m. are reported for each experimental group.

Acknowledgements

We thank Sara Moberg for comments on the manuscript. We also thank Carine Moigneu for viral injections, Julien Grimaud and Lucie Dixsaut for early works. We also wish to thank Uwe Maskos and David DiGregorio from the Institut Pasteur for the gift of SST-Cre, PV-Cre and VIP-Cre mice. We also thank the Genetically-Encoded Neuronal Indicator and Effector (GENIE) Project and the Janelia Farm Research Campus of the Howard Hughes Medical Institute for sharing GCaMP6f constructs .This work was supported by the life insurance company “AG2R-La-Mondiale”, the Agence Nationale de la Recherche (ANR-15-CE37-0004 “SmellBrain” and ANR-16-CE37-0010 “ORUPS”) and the Laboratoire d'Excellence Revive (Investissement d'Avenir, ANR-10-LABX-73). Our laboratory is part of the Ecole des Neurosciences de Paris (ENP) Ile-de-France network and is affiliated with the *Bio-Psy* Laboratory of Excellence. C.M. is a recipient of a fellowship from the French Ministère de l’Education Supérieure et de la Recherche and was also supported by the Fondation de la Recherche Médicale (FDT20160435483). S.S. acknowledges funding from the ENP Graduate program and the Labex Revive consortium for his doctoral program. C.M. and S.S acknowledge the ED3C doctoral school of the Sorbonne Université.

Author contributions

C.M., G.L., A.N., S.S. and P.-M.L. designed the experiments, C.M., G.L., A.N., S.S., and E.P. performed and analyzed the experiments. C.M., G.L., S.S. and P.-M.L. wrote the manuscript.

Competing interests

The authors declare no competing interests.

Data availability

The datasets generated during the current study as well as the custom MATLAB code used to analyze the data are available from the corresponding authors upon reasonable request.

References

1. Seress, L. & Ribak, C. E. GABAergic cells in the dentate gyrus appear to be local circuit and projection neurons. *Exp. Brain Res.* **50**, 173–182 (1983).

2. Freund, T. F. & Antal, M. GABA-containing neurons in the septum control inhibitory interneurons in the hippocampus. *Nature* **336**, 170–173 (1988).

3. Tóth, K., Borhegyi, Z. & Freund, T. F. Postsynaptic targets of GABAergic hippocampal neurons in the medial septum-diagonal band of broca complex. *J. Neurosci.* **13**, 3712–3724 (1993).

4. Tomioka, R. *et al.* Demonstration of long-range GABAergic connections distributed throughout the mouse neocortex. *Eur. J. Neurosci.* **21**, 1587–1600 (2005).

5. Tomioka, R. & Rockland, K. S. Long-distance corticocortical GABAergic neurons in the adult monkey white and gray matter. *J. Comp. Neurol.* **505**, 526–538 (2007).

6. Higo, S. Subtypes of GABAergic neurons project axons in the neocortex. *Front. Neuroanat.* **3**, 25 (2009).

7. Higo, S., Udaka, N. & Tamamaki, N. Long-range GABAergic projection neurons in the cat neocortex. *J. Comp. Neurol.* **503**, 421–431 (2007).

8. McDonald, C. T. & Burkhalter, A. Organization of long-range inhibitory connections within rat visual cortex. *J. Neurosci.* **13**, 768–781 (1993).

9. Tamamaki, N. & Tomioka, R. Long-range GABAergic connections distributed throughout the neocortex and their possible function. *Front. Neurosci.* **4**, 1–8 (2010).

10. Caputi, A., Melzer, S., Michael, M. & Monyer, H. The long and short of GABAergic neurons. *Curr. Opin. Neurobiol.* **23**, 179–86 (2013).

11. Melzer, S. *et al.* Long-Range-Projecting GABAergic Neurons Modulate Inhibition in Hippocampus and Entorhinal Cortex. *Science (80-.).* **335**, 1506–1510 (2012).

12. M. He et al. Strategies and tools for combinatorial targeting of GABAergic neurons in mouse cerebral cortex. Neuron. 2016 Sep 21; 91(6): 1228–1243.

13. Christenson Wick, Z., Tetzlaff, M. R. & Krook-Magnuson, E. Novel long-range inhibitory nNOS-expressing hippocampal cells. *Elife* **8**, (2019).

14. Jinno, S. & Kosaka, T. Parvalbumin is expressed in glutamatergic and GABAergic corticostriatal pathway in mice. *J. Comp. Neurol.* **477**, 188–201 (2004).

15. Lee, A. T., Vogt, D., Rubenstein, J. L. & Sohal, V. S. A class of GABAergic neurons in the prefrontal cortex sends long-range projections to the nucleus accumbens and elicits acute avoidance behavior. *J. Neurosci.* **34**, 11519–25 (2014).

16. Rock, C., Zurita, H., Lebby, S., Wilson, C. J. & Apicella, A. junior. Cortical Circuits of Callosal GABAergic Neurons. *Cereb. Cortex* 1–14 (2017). doi:10.1093/cercor/bhx025

17. Zurita, H., Feyen, P. L. C. & Apicella, A. J. Layer 5 Callosal Parvalbumin-Expressing Neurons: A Distinct Functional Group of GABAergic Neurons. *Front. Cell. Neurosci.* **12**, 53 (2018).

18. Francavilla, R. *et al.* Connectivity and network state-dependent recruitment of long-range VIP-GABAergic neurons in the mouse hippocampus. *Nat. Commun.* **9**, 1–17 (2018).

19. Melzer, S. *et al.* Distinct Corticostriatal GABAergic Neurons Modulate Striatal Output Neurons and Motor Activity. *Cell Rep.* **19**, 1045–1055 (2017).

20. Klausberger, T. & Somogyi, P. Neuronal diversity and temporal dynamics: the unity of hippocampal circuit operations. *Science* **321**, 53–7 (2008).

21. Bertero, A., Feyen, P. L. C., Zurita, H. & Apicella, A. J. A Non-Canonical Cortico-Amygdala Inhibitory Loop. *J. Neurosci.* **39**, 8424–8438 (2019).

22. Rock, C., Zurita, H., Wilson, C. & Apicella, A. J. An inhibitory corticostriatal pathway. *Elife* **5**, (2016).

23. Gilbert, C. D. & Li, W. Top-down influences on visual processing. **14**, 350–363 (2013).

24. Keller, G. B. & Mrsic-flogel, T. D. Perspective Predictive Processing : *Neuron* **100**, 424–435 (2018).

25. Isaacson, J. S. & Scanziani, M. How inhibition shapes cortical activity. *Neuron* **72**, 231–43 (2011).

26. Eyre, M. D., Antal, M. & Nusser, Z. Distinct deep short-axon cell subtypes of the main olfactory bulb provide novel intrabulbar and extrabulbar GABAergic connections. *J. Neurosci.* **28**, 8217–29 (2008).

27. Sonoda, T. *et al.* A noncanonical inhibitory circuit dampens behavioral sensitivity to light. *Science (80-.).* **368**, 527 LP – 531 (2020).

28. de Olmos, J., Hardy, H. & Heimer, L. The afferent connections of the main and the accessory olfactory bulb formations in the rat: an experimental HRP-study. *J. Comp. Neurol.* **181**, 213–244 (1978).

29. Haberly, L. B. & Price, J. L. Association and commissural fiber systems of the olfactory cortex of the rat. I. Systems originating in the piriform cortex and dajacent areas. *J. Comp. Neurol.* **178**, 711–40 (1978).

30. Haberly, L. B. & Price, J. L. Association and Commissural Fiber Systems of the Olfactory Cortex of the Rat. II Systems originating in the olfactory peduncle. *J. Comp. Neurol.* 781–807 (1978).

31. Davis, B. J. & Macrides, F. The Organization of Centrifugal Projections From the Anterior Olfactory Nucleus, Ventral Hippocampal Rudiment, and Piriform Cortex to the Main Olfactory Bulb in the

Hamster : An Autoradiograpic Study. *J. Comp. Neurol.* **493**, 475–493 (1981).

32. Luskin, M. B. & Price, J. L. The topographic organization of associational fibers of the olfactory system in the rat, including centrifugal fibers to the olfactory bulb. *J. Comp. Neurol.* **216**, 264–291 (1983).

33. Carson, K. a. Quantitative localization of neurons projecting to the mouse main olfactory bulb. *Brain Res. Bull.* **12**, 635–9 (1984).

34. Shipley, M. T. & Adamek, G. D. The connections of the mouse olfactory bulb: A study using orthograde and retrograde transport of wheat germ agglutinin conjugated to horseradish peroxidase. *Brain Res. Bull.* **12**, 669–688 (1984).

35. Markopoulos, F., Rokni, D., Gire, D. H. & Murthy, V. N. Functional properties of cortical feedback projections to the olfactory bulb. *Neuron* **76**, 1175–88 (2012).

36. Boyd, A. M., Sturgill, J. F., Poo, C. & Isaacson, J. S. Cortical feedback control of olfactory bulb circuits. *Neuron* **76**, 1161–74 (2012).

37. Padmanabhan, K. *et al.* Diverse Representations of Olfactory Information in Centrifugal Feedback Projections. *J. Neurosci.* **36**, 7535–45 (2016).

38. Mazo, C., Grimaud, J., Shima, Y., Murthy, V. N. & Lau, C. G. Distinct projection patterns of different classes of layer 2 principal neurons in the olfactory cortex. *Sci Rep* **7,** 8282 (2017).

39. Mazo, C., Lepousez, G., Nissant, A., Valley, M. T. & Lledo, P.-M. P.-M. GABAB Receptors Tune Cortical Feedback to the Olfactory Bulb. *J. Neurosci.* **36**, 8289–8304 (2016).

40. Alonso, M. *et al.* Activation of adult-born neurons facilitates learning and memory. *Nat. Neurosci.* **2**, 1–10 (2012).

41. Nissant, A., Bardy, C., Katagiri, H., Murray, K. & Lledo, P.-M. Adult neurogenesis promotes synaptic plasticity in the olfactory bulb. *Nat. Neurosci.* **12**, 728–30 (2009).

42. Martin, C., Gervais, R., Messaoudi, B. & Ravel, N. Learning-induced oscillatory activities correlated to odour recognition: a network activity. *Eur. J. Neurosci.* **23**, 1801–10 (2006).

43. Kay, L. M. *Circuit oscillations in odor perception and memory*. *Progress in Brain Research* **208**, (Elsevier B.V., 2014).

44. Otazu, G. H., Chae, H., Davis, M. B. & Albeanu, D. F. Cortical Feedback Decorrelates Olfactory Bulb Output in Awake Mice. *Neuron* 1–17 (2015). doi:10.1016/j.neuron.2015.05.023

45. Grobman, M. *et al.* A Mirror-Symmetric Excitatory Link Coordinates Odor Maps across Olfactory Bulbs and Enables Odor Perceptual Unity. *Neuron* **99**, 800-813.e6 (2018).

46. Soria-Gómez, E. *et al.* The endocannabinoid system controls food intake via olfactory processes. *Nat. Neurosci.* **17**, 407–15 (2014).

47. Wang, C. Y., Liu, Z., Ng, Y. H. & Südhof, T. C. A Synaptic Circuit Required for Acquisition but Not Recall of Social Transmission of Food Preference. *Neuron* 1–14 (2020). doi:10.1016/j.neuron.2020.04.004

48. Wu, A. *et al.* Context-dependent plasticity of adult-born neurons regulated by cortical feedback. *Sci. Adv.* **6**, eabc8319 (2020).

49. Zaborszky, L., Carlsen, J., Brashear, H. R. & Heimer, L. Cholinergic and Gabaaergic Afferents to the Olfactory-Bulb in the Rat with Special Emphasis on the Projection Neurons in the Nucleus of the Horizontal Limb of the Diagonal Band. *J. Comp. Neurol.* **243**, 488-509. (1986).

50. Kunze, W. a, Shafton, a D., Kemm, R. E. & McKenzie, J. S. Olfactory bulb output neurons excited from a basal forebrain magnocellular nucleus. *Brain Res* **583**, 327–331 (1992).

51. Kunze, W. A. A., Shafton, A. D., Kemm, R. E. & McKenzie, J. S. Intracellular responses of olfactory bulb granule cells to stimulating the horizontal diagonal band nucleus. *Neuroscience* **48**, 363–369 (1992).

52. Gracia-Llanes, F. J. *et al.* GABAergic basal forebrain afferents innervate selectively GABAergic targets in the main olfactory bulb. *Neuroscience* **170**, 913–922 (2010).

53. Nunez-Parra, A., Maurer, R. K., Krahe, K., Smith, R. S. & Araneda, R. C. Disruption of centrifugal inhibition to olfactory bulb granule cells impairs olfactory discrimination. *Proc. Natl. Acad. Sci. U. S. A.* **2013**, 1–3 (2013).

54. Diez, A. S., Najac, M. & D. De Saint Jan. Basal forebrain GABAergic innervation of olfactory bulb periglomerular interneurons. J Physiol. 2019 May;597(9):2547-2563. doi: 10.1113/JP277811. Epub 2019 Apr 8.

55. Villar, P., Hu, R. & Araneda, R. Long-range GABAergic inhibition modulates spatiotemporal dynamics of the output neurons in the olfactory bulb. *bioRxiv* 2020.07.08.194324 (2020). doi:10.1101/2020.07.08.194324

56. Kay, R. B. & Brunjes, P. C. Diversity among principal and GABAergic neurons of the anterior olfactory nucleus. *Front. Cell. Neurosci.* **8**, 111 (2014).

57. Suzuki, N. & Bekkers, J. M. Inhibitory neurons in the anterior piriform cortex of the mouse: classification using molecular markers. *J. Comp. Neurol.* **518**, 1670–1687 (2010).

58. Klapoetke, N. C. *et al.* Independent optical excitation of distinct neural populations. *Nat. Methods* **11**, (2014).

59. Wang, D. *et al.* Improved Separation of Odor Responses in Granule Cells of the Olfactory Bulb During Odor Discrimination Learning. *Front. Cell. Neurosci.* **14**, 579349 (2020).

60. Lin, J. Y., Lin, M. Z., Steinbach, P. & Tsien, R. Y. Characterization of engineered channelrhodopsin variants with improved properties and kinetics. *Biophys. J.* **96**, 1803–14 (2009).

61. Kikuta, S., Fletcher, M. L., Homma, R., Yamasoba, T. & Nagayama, S. Odorant Response Properties of Individual Neurons in an Olfactory Glomerular Module. *Neuron* **77**, 1122–1135 (2013).

62. Adam, Y. Functional transformations of odor inputs in the mouse olfactory bulb. *Front. Neural Circuits* **8**, 129 (2014).

63. Yamada, Y. *et al.* Context- and Output Layer-Dependent Long-Term Ensemble Plasticity in a Sensory Circuit. *Neuron* 1–15 (2017). doi:10.1016/j.neuron.2017.02.006

64. Ait Ouares, K., Beurrier, C., Canepari, M., Laverne, G. & Kuczewski, N. Opto nongenetics inhibition of neuronal firing. *Eur. J. Neurosci.* **49**, 6–26 (2019).

65. Wachowiak, M. *et al.* Optical dissection of odor information processing in vivo using GCaMPs expressed in specified cell types of the olfactory bulb. *J. Neurosci.* **33**, 5285–300 (2013).

66. Economo, M. N., Hansen, K. R. & Wachowiak, M. Control of Mitral/Tufted Cell Output by Selective Inhibition among Olfactory Bulb Glomeruli. *Neuron* **91**, 397–411 (2016).

67. Banerjee, A. *et al.* An Interglomerular Circuit Gates Glomerular Output and Implements Gain Control in the Mouse Olfactory Bulb. *Neuron* **87**, 193–207 (2015).

68. Lepousez, G. & Lledo, P.-M. Odor discrimination requires proper olfactory fast oscillations in awake mice. *Neuron* **80**, 1010–1024 (2013).

69. Buzsáki, G. & Wang, X.-J. Mechanisms of Gamma Oscillations. *Annu. Rev. Neurosci.* **35**, 203–225 (2012).

70. Davis, B. J., Macrides, F., Youngs, W. M., Schneider, S. P. & Rosene, D. L. Efferents and centrifugal

afferents of the main and accessory olfactory bulbs in the hamster. *Brain Res. Bull.* **3**, 59–72 (1978).

71. de Olmos, J., Hardy, H. & Heimer, L. The afferent connections of the main and the accessory olfactory bulb formations in the rat: an experimental HRP-study. *J. Comp. Neurol.* **181**, 213–244 (1978).

72. Miyamichi, K. *et al.* Dissecting local circuits: parvalbumin interneurons underlie broad feedback control of olfactory bulb output. *Neuron* **80**, 1232–45 (2013).

73. Diodato, A. *et al.* Molecular signatures of neural connectivity in the olfactory cortex. *Nat. Commun.* **7**, 1–10 (2016).

74. Guo, W., Clause, A. R., Barth-Maron, A. & Polley, D. B. A Corticothalamic Circuit for Dynamic Switching between Feature Detection and Discrimination. *Neuron* **95**, 180-194.e5 (2017).

75. Martin, C. & Ravel, N. Beta and gamma oscillatory activities associated with olfactory memory tasks: different rhythms for different functional networks? *Front. Behav. Neurosci.* **8**, 1–13 (2014).

76. Smear, M., Resulaj, A., Zhang, J., Bozza, T. & Rinberg, D. Multiple perceptible signals from a single olfactory glomerulus. *Nat. Neurosci.* **16**, 1687–91 (2013).

77. Smear, M., Shusterman, R., O'Connor, R., Bozza, T. & Rinberg, D. Perception of sniff phase in mouse olfaction. *Nature* **479**, 397–400 (2011).

78. Shusterman, R., Smear, M. C., Koulakov, A. a & Rinberg, D. Precise olfactory responses tile the sniff cycle. *Nat. Neurosci.* **14**, 1039–1044 (2011).

79. Fukunaga, I., Berning, M., Kollo, M., Schmaltz, A. & Schaefer, A. T. Two distinct channels of olfactory bulb output. *Neuron* **75**, 320–9 (2012).

80. Gschwend, O., Beroud, J. & Carleton, A. Encoding odorant identity by spiking packets of rate-invariant neurons in awake mice. *PLoS One* **7**, e30155 (2012).

81. Li, A., Gire, D. H. & Restrepo, D. Spike-Field Coherence in a Population of Olfactory Bulb Neurons Differentiates between Odors Irrespective of Associated Outcome. *J. Neurosci.* **35**, 5808–5822 (2015).

82. Gschwend, O. *et al.* Neuronal pattern separation in the olfactory bulb improves odor discrimination learning. *Nat. Neurosci.* **18**, 1474–82 (2015).

83. Haberly, L. B. & Price, J. L. The axonal projection patterns of the mitral and tufted cells of the olfactory bulb in the rat. *Brain Res.* **129**, 152–157 (1977).

84. Igarashi, K. M. *et al.* Parallel Mitral and Tufted Cell Pathways Route Distinct Odor Information to Different Targets in the Olfactory Cortex. *J. Neurosci.* **32**, 7970–7985 (2012).

85. Young, H., Belbut, B., Baeta, M. & Petreanu, L. Laminar-specific cortico-cortical loops in mouse visual cortex. *bioRxiv* **4**, 773085 (2019).

86. Kim, E. J. *et al.* Extraction of Distinct Neuronal Cell Types from within a Genetically Continuous Population. *Neuron* **107**, 1–9 (2020).

87. Hanson, E., Swanson, J. & Arenkiel, B. R. GABAergic Input From the Basal Forebrain Promotes the Survival of Adult-Born Neurons in the Mouse Olfactory Bulb. *Front. Neural Circuits* **14**, 17 (2020).

88. Böhm, E., Brunert, D. & Rothermel, M. Input dependent modulation of olfactory bulb activity by GABAergic basal forebrain projections. doi:10.1101/2020.03.29.014191

89. Crandall, S. R., Cruikshank, S. J. & Connors, B. W. A Corticothalamic Switch: Controlling the Thalamus with Dynamic Synapses. *Neuron* **86**, 768–782 (2015).

90. Kirchgessner, M. A., Franklin, A. D. & Callaway, E. M. Context-dependent and dynamic functional influence of corticothalamic pathways to first- and higher-order visual thalamus. *Proc. Natl. Acad. Sci. U. S. A.* 1–12 (2020). doi:10.1073/pnas.2002080117

91. Halassa, M. M. & Acsády, L. Thalamic Inhibition: Diverse Sources, Diverse Scales. *Trends Neurosci.* **39**, 680–693 (2016).

92. Basu, J. *et al.* Gating of hippocampal activity, plasticity, and memory by entorhinal cortex long-range inhibition. *Science (80-.).* **351**, aaa5694–aaa5694 (2016).

93. Hayar, A., Karnup, S., Ennis, M. & Shipley, M. T. External tufted cells: a major excitatory element that coordinates glomerular activity. *J. Neurosci.* **24**, 6676–85 (2004).

94. Murphy, G. J., Darcy, D. P. & Isaacson, J. S. Intraglomerular inhibition: signaling mechanisms of an olfactory microcircuit. *Nat. Neurosci.* **8**, 354–64 (2005).

95. Gunaydin, L. a *et al.* Natural neural projection dynamics underlying social behavior. *Cell* **157**, 1535–51 (2014).

96. Adam, Y. *et al.* Functional transformations of odor inputs in the mouse olfactory bulb. *Front. Neural Circuits* **8**, 129 (2014).

97. Dubbs, A., Guevara, J. & Yuste, R. moco: Fast Motion Correction for Calcium Imaging. *Front. Neuroinform.* **10**, 6 (2016).

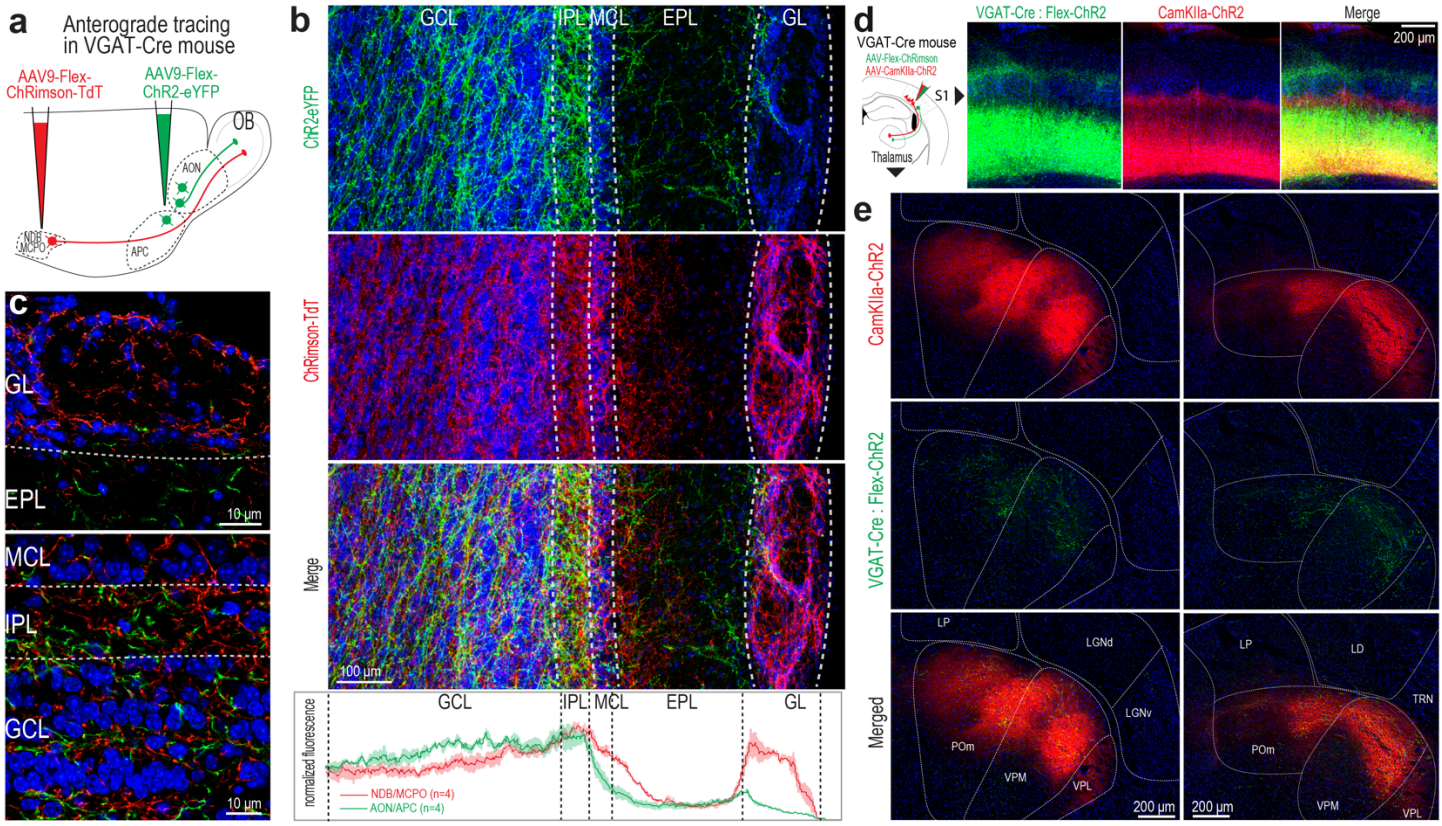

Figure 1. The olfactory cortex sends GABAergic projections back to the OB. a, Comparative anterograde labeling of NDB/MCPO (ChRimson-TdTomato) versus AON/APC (ChR2-eYFP) GABAergic axons in the OB using Cre-dependent AAV injection in VGAT-Cre mice. **b**, Confocal images exhibiting the laminar profile of OB innervation by GABAergic axons from the AON/APC (top, green) or NDB/MCPO (middle, red). Bottom, merge. Blue, DAPI. Bottom plot, normalized axon fluorescence intensity from NDB/MCPO (red) vs. AON/APC (green) across dorsal OB layers. Mean (solid line) ± sem (shaded). n = 4 mice. GL, glomerular Layer; EPL, external plexiform layer; MCL, mitral cell layer; IPL, internal plexiform layer; GCL, granule cell layer. **c**, Higher confocal magnification of B in the different OB layers. **d**, Anterograde labeling of S1 glutamatergic (AAV9-CamKIIa-ChR2) and GABAergic (AAV9-FLEX-ChRimson) axons in the sensory thalamic nuclei. Right, Injection site in L5/6 of S1, barrel field. Blue, DAPI. **e**, Glutamatergic (red) and GABAergic (green) axons across 2 sections from 2 individuals through the sensory thalamic nuclei. Blue, DAPI. Thalamic nuclei: LD: latero-dorsal LP: lateral posterior; POm: posteriomedial; VPL: ventral posterolateral; VPM: medial ventral posteriomedial; TRN: thalamic reticular nucleus.

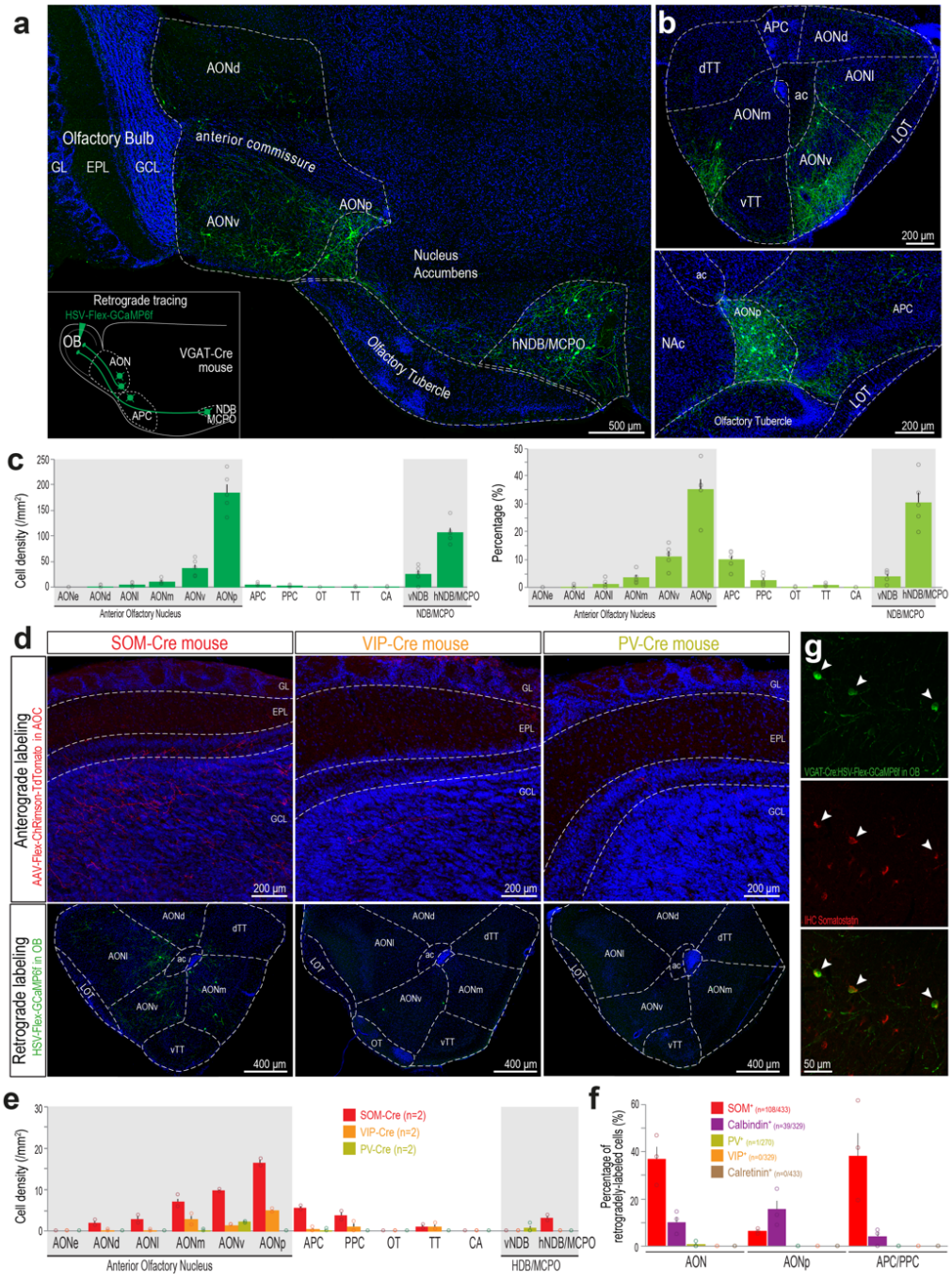

Figure 2. Anatomical and neurochemical identification of the OB-projecting GABAergic cells in the olfactory cortex. a, OB-projecting GABAergic cells in a sagittal slice. Inset: schematic of the injection. AONd, AON dorsalis; AONv, AON ventralis; AONp, AON posterioralis; hNDB/MCPO, horizontal limb of the nucleus of the diagonal band / magnocellular preoptic nucleus; vNDB, vertical limb of the nucleus of the diagonal band. **b**, Coronal slices through the AON (top) and APC (bottom). AONl: AON lateralis; AONm,

AON medialis; dTT, dorsal Tenia Tecta; vTT, ventral Tenia Tecta; LOT, lateral olfactory tract; NAc, nucleus accumbens; ac, anterior commissure. **c,** Cell density (left) and relative proportion (right) of the OB-projecting GABAergic cells (n = 5 mice). Data presented as mean ± sem; circle, individual mice. OT: olfactory tubercle; CA: cortical amygdala; vNDB, vertical limb of diagonal band nucleus. **d**, Top, anterograde labeling of SOM-, VIP- and PV-axons in the OB (ChR2-tdTomato). Sagittal sections through the OB. Bottom, retrograde labeling of OB-projecting cells (GCaMP6f) in SOM-, VIP- and PV-Cre mice. Coronal sections through the AON. **e**, Cell density of the retrogradely-labeled cells in SOM-Cre (red; n = 2 mice), VIP-Cre (orange; n = 2 mice) and PV-Cre (green; n = 2 mice). Data presented as mean ± sem; circle, individual mice. **f**, Quantification of co-labeled cells across olfactory cortical regions with different interneuronal markers. Data presented as mean ± sem; circle, individual mice (n = 3 mice). The total number of analyzed retrogradely-labeled cells and co-labeled cells are respectively indicated for each marker. **g**, Example SOM labeling (immunohistochemistry, IHC) of OB-projecting neurons in the AON. Arrowheads point to co-labeled cells.

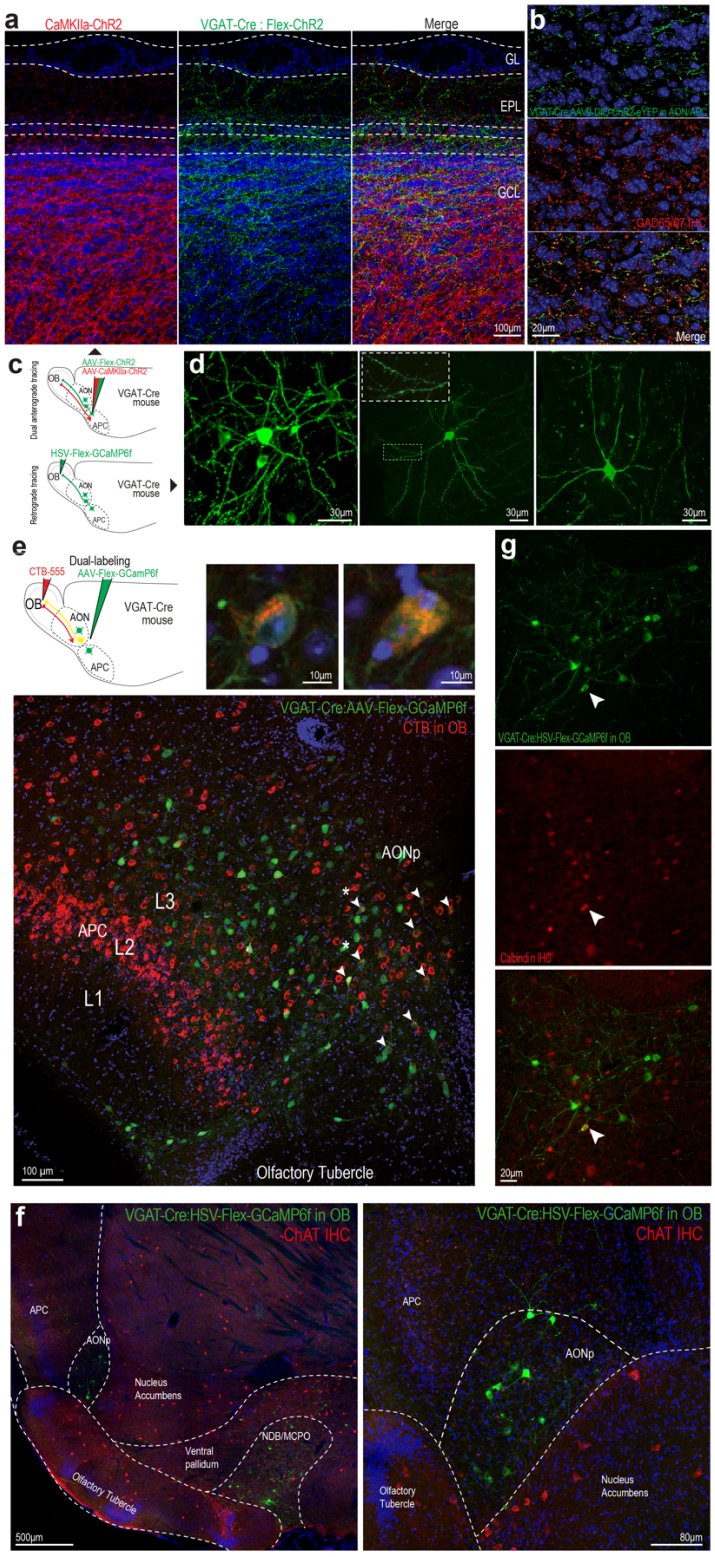

Extended Data Fig. 1. Complementary anatomical and neurochemical analysis of the OB-projecting GABAergic cells in the AON/APC. **a**, Anterograde labeling of glutamatergic (left, ChR2-mCherry) and

GABAergic (middle, ChR2-eYFP) axons from the AON/APC of VGAT-Cre mice. Right, merge. Blue, DAPI. **b**, High magnification of the GCL of VGAT-Cre mice injected with AAV-Flex-ChR2-eYFP in the AON/APC (top). Middle, IHC against the GABA-synthesizing enzymes GAD65 and GAD67. Bottom, co-labeling of the cortical projections with GAD65 and GAD67 staining, confirming the GABAergic nature of the axons. Blue, DAPI. **c**, Schematic of the dual labeling of glutamatergic and GABAergic AOC projections to the OB (top, related to panel (a)) and retrograde labeling of OB-projecting GABAergic neurons (bottom, related to panel (d)). **d**, Examples of retrogradely-labeled cells. Middle and right panels show spiny (see inset, detail of the boxed region) and unspiny neurons from the AON/APC. **e**, Non-selective retrograde labeling of OB-projecting cells (CTB-555) and viral neuronal labeling of GABAergic neurons recapitulate the observations with HSV. Bottom, coronal slice through the APC/AONp (1.7 mm anterior to Bregma). CTB produced a classic labeling of cortico-bulbar glutamatergic cells in L2 and L3 in the APC. Double-labeled cells (arrowheads) were mainly found in the AONp, located at the border between the APC and OT. Starred cells are magnified in the top panels. Blue, DAPI. **f**, Choline acetyltransferase (ChAT) IHC in the AONp showing that retro-labeled cells are located outside the cholinergic-rich brain area. Compare with cells in the NDB/MCPO. This argues against the hypothesis that this region is a rostral extension of a striatal or pallidal structure. Blue, DAPI. **g**, IHC against Calbindin showing a double-labeled cell (arrowhead) in the AONp.

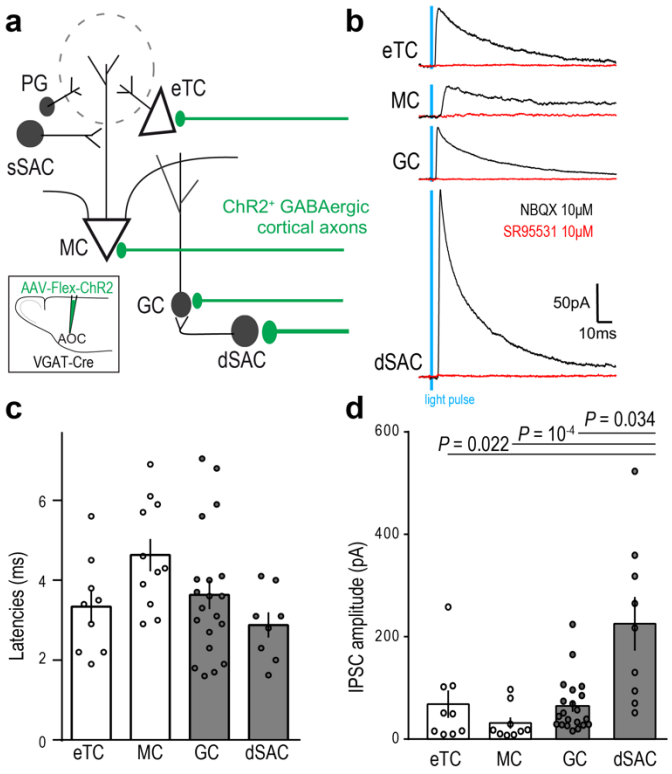

Figure 3. Cortico-bulbar GABAergic axons form functional synapses with inhibitory and excitatory neurons in the OB. **a**, Recording schematic. Periglomerular (PG) cells, external tufted cells (eTCs), superficial short-axon cells (sSAC), mitral cells (MCs), granule cells (GCs) and deep short-axon cells (dSACs) were patched (whole-cell) and GABAergic feedback axons expressing ChR2 were light-stimulated (inset). Width of the axon shafts indicates connection probability. **b**, Representative example traces of cells recorded at 0 mV. Blue: light-pulse (1 ms), black, recordings in NBQX (10 µM); red, recordings in SR95531 (10 µM). **c-d**, IPSC latencies (**c**) and amplitudes (**d**) in the cells receiving direct inputs (One-way ANOVA with Tukey's post-hoc test; eTC, n =9 cells; MC, n =11; GC, n =21; dSAC, n =9). White bars, excitatory neurons; Gray bars, inhibitory neurons; circle, individual cell. Data presented as mean ± sem.

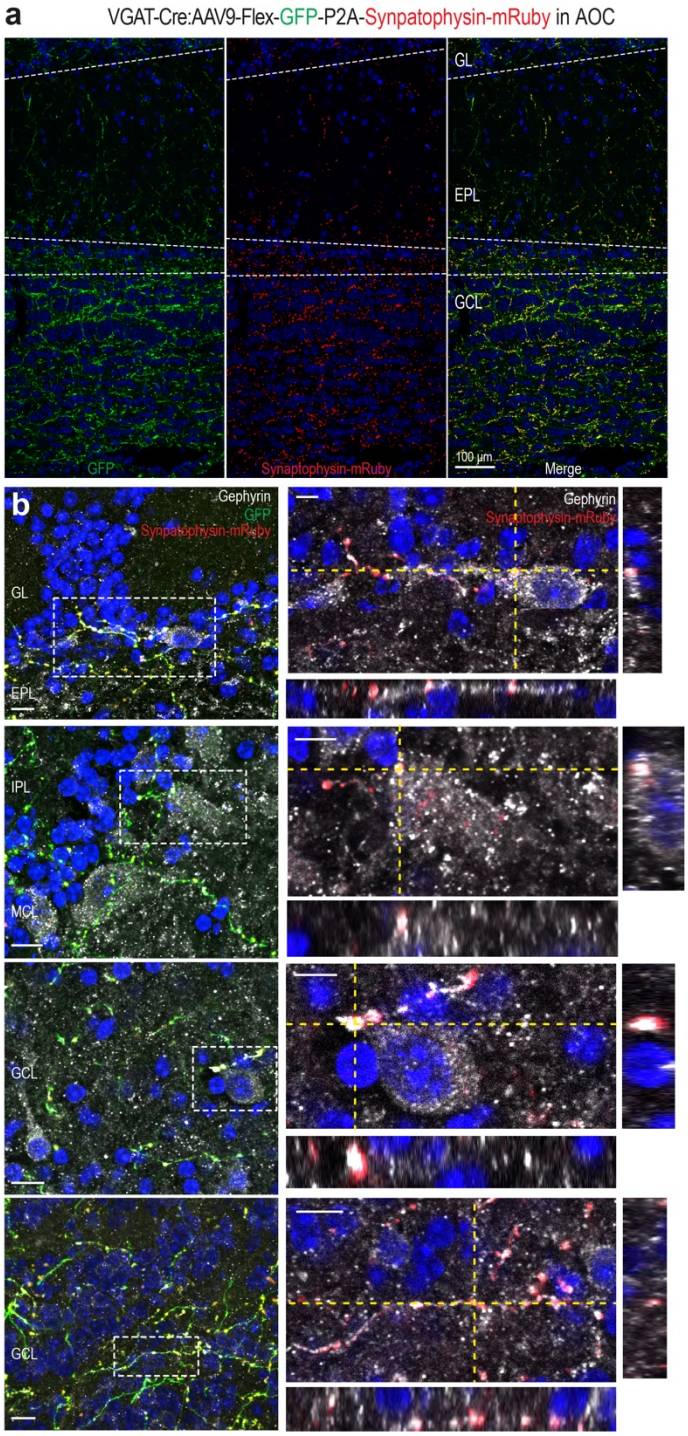

Extended Data Fig. 2. Putative GABAergic synapses between AON/APC axons and OB neurons. a, Anterograde labeling of cortical GABAergic axons (shaft, green) and their putative presynaptic component (red) across OB layers. **b**, Close apposition of putative pre- and post-synaptic sites (synaptophysin, red and gephyrin, white, respectively). GFP, axon shaft; Blue, DAPI. Scale bars, 10 µm. Right, z-stack projection of

the synaptophysin and gephyrin channels (DAPI, single plane) of the boxed region in the left image. Yellow dashed crosshair depicts the planes for the orthogonal views located in the right and bottom excerpts. From top to bottom: presumed JG cells at the transition between GL and EPL (top); putative MC in the MCL (middle); putative dSAC and axons in the GCL (bottom two). Scale bars, 5 µm.

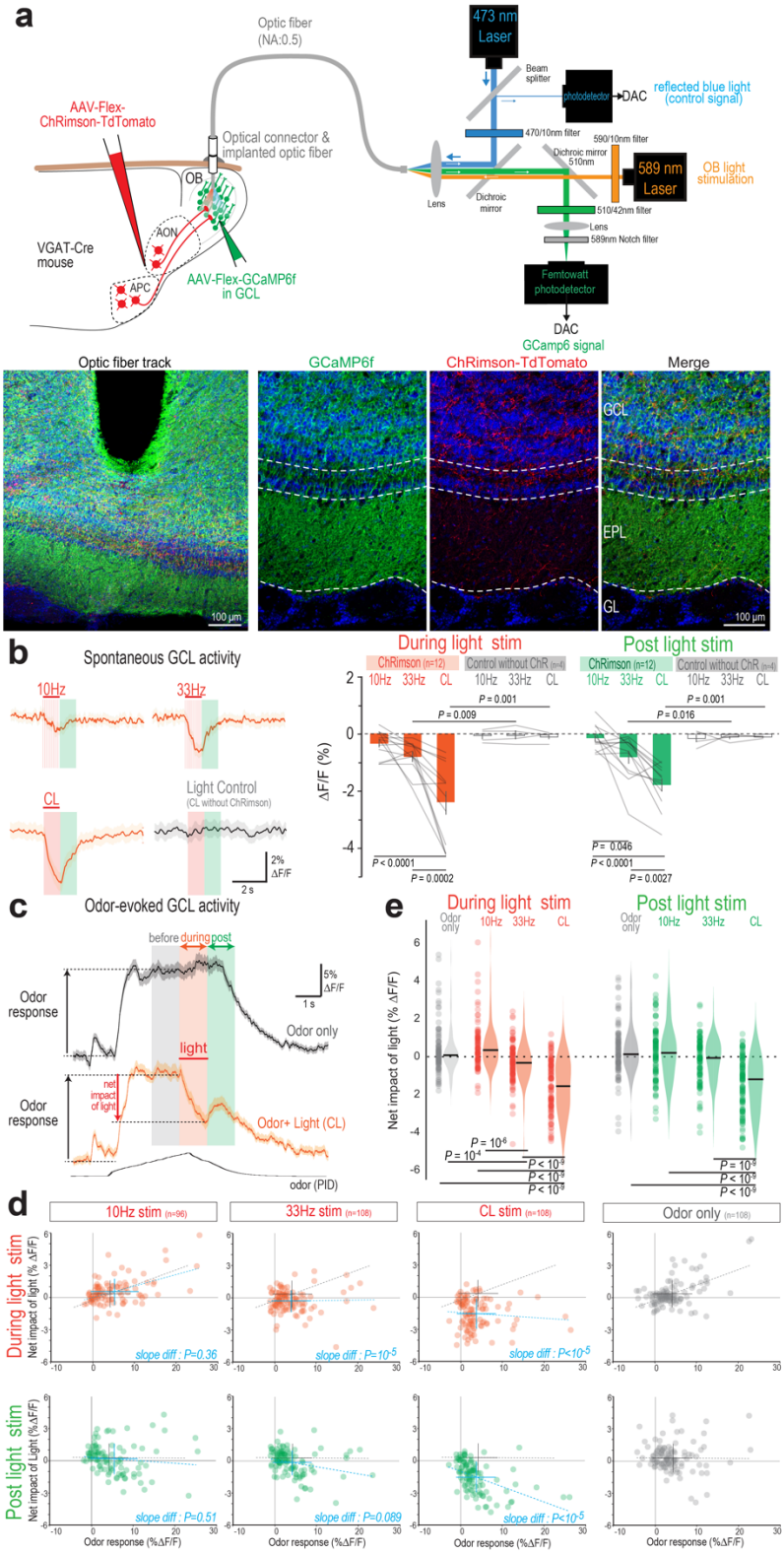

Figure 4. Cortico-bulbar GABAergic axons induce net inhibition onto GCL neurons *in vivo*. a, Schematic of the light path for fiber photometry and optogenetic stimulation in the OB (top). Bottom, images

showing the optic fiber tract, GCaMP6f expression across OB layers and ChRimson in AON/APC GABAergic axons. Blue, DAPI. **b**, Example spontaneous fluorescence responses to light stimulation (averages over 20 trails). “Light control” is light illumination in mice lacking ChRimson expression (gray, n = 4 recording sites in 2 mice). Right, Stimulation at 33Hz and CL, but not at 10 Hz, induced a significant change in mean fluorescence (RM-One-way-ANOVA, $F(2,22)=21.28$, $P<0.0001$). This effect was also observed during the 1 s period post-light (RM-One-way-ANOVA, $F(2,22)=20.64$, $P<0.0001$). Data presented as mean ± sem; gray lines, individual mice. **c**, Fluorescence signals during odor presentation only (black) and light stimulation coupled to odor presentation (orange, mean ± sem). The “net impact of light” represents the mean fluorescence change during light relative to the odor response magnitude measured just before light. **d**, Net impact of light as a function of odor response magnitude during (red) or 1s after (green) stimulation. Dashed line, linear regression; cross, average response ± sem. 33 Hz and CL, but not 10 Hz light stimulation, produced a significant change of the odor-evoked response and in the slope of correlation (blue dashed line) compared to the “odor-only” condition (gray dashed line; ANCOVA). This effect persisted 1s after light stimulation. **e**, Net impact of light on odor responses across light stimulation protocols (10 Hz, 33 Hz, CL) compared to no light stimulation (“odor only”), during (left, orange) and after (right, green) light stimulation. Population odor response inhibition correlated with the stimulation strength during light stimulation (One-way-ANOVA with Tukey’s post-hoc test). After light stimulation offset, only CL caused greater inhibition than any other light pattern. Violin plots are ks density estimates; black bar is median; circle, individual odor-recording site pair.

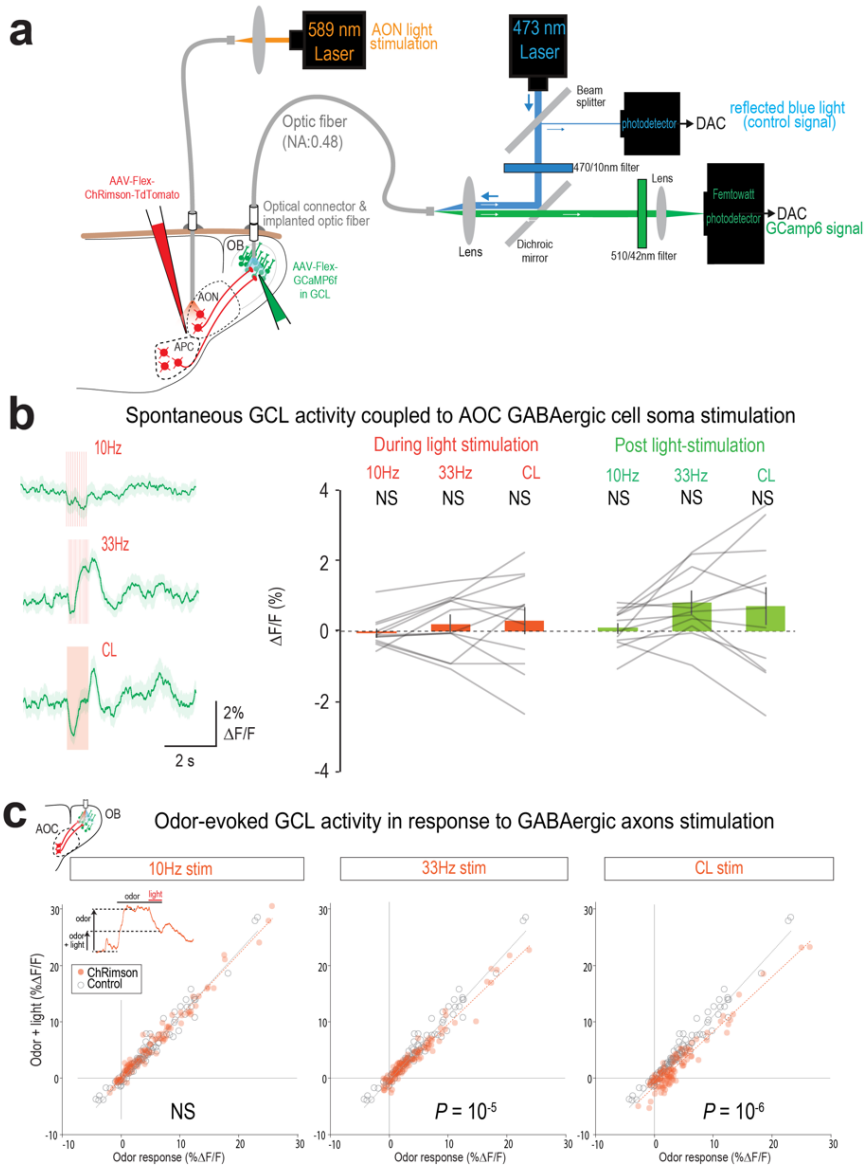

Extended Data Fig. 3. Complementary analysis of the cortico-bulbar inhibition of GCL neurons. a, Schematic of the light path for fiber photometry in the OB and optogenetic stimulation in the AON. Spontaneous activity in GCL GABAergic neurons was continuously recorded and cortical GABAergic neurons were light stimulated utilizing an optic fiber implanted in the AON. **b**, Representative averaged traces of GCL neuronal responses to cortical GABAergic neuron somas stimulation at 10 Hz, 33 Hz or with CL (orange shaded area; left). Right, Variable but not significant changes of the light-evoked responses during (orange) and 1 s after (green) stimulation (n =12 recording sites, 8 mice; RM-One-Way-ANOVA, during stim, $F(2,22)=0.83$, $P=0.44$; post-stim, $F(2,22)=2.42$, $P=0.11$, Tukey's post-hoc, NS). Data presented

as mean ± sem. Gray lines, individual mice. **c**, Left, Stimulation of cortical GABAergic axons. Right, Odor responses during light stimulation period as a function of odor responses before stimulation. Orange, ChRimson stimulation at 10Hz, 33Hz, or with CL. Gray, control without light stimulation. Circle, individual recording-odor pairs. Significant change of the slopes for 33 Hz and CL (ANOVA; n = 108 odor-recording pairs for odor-only, 33 Hz and CL; n = 96 for 10 Hz). Slope: control, 1.14 ± 0.021, R^2=0.96; 10Hz, 1.11 ± 0.019, R^2=0.97; 33Hz, 1.01 ± 0.021, R^2=0.95; CL, 0.98 ± 0.028, R^2=0.91.

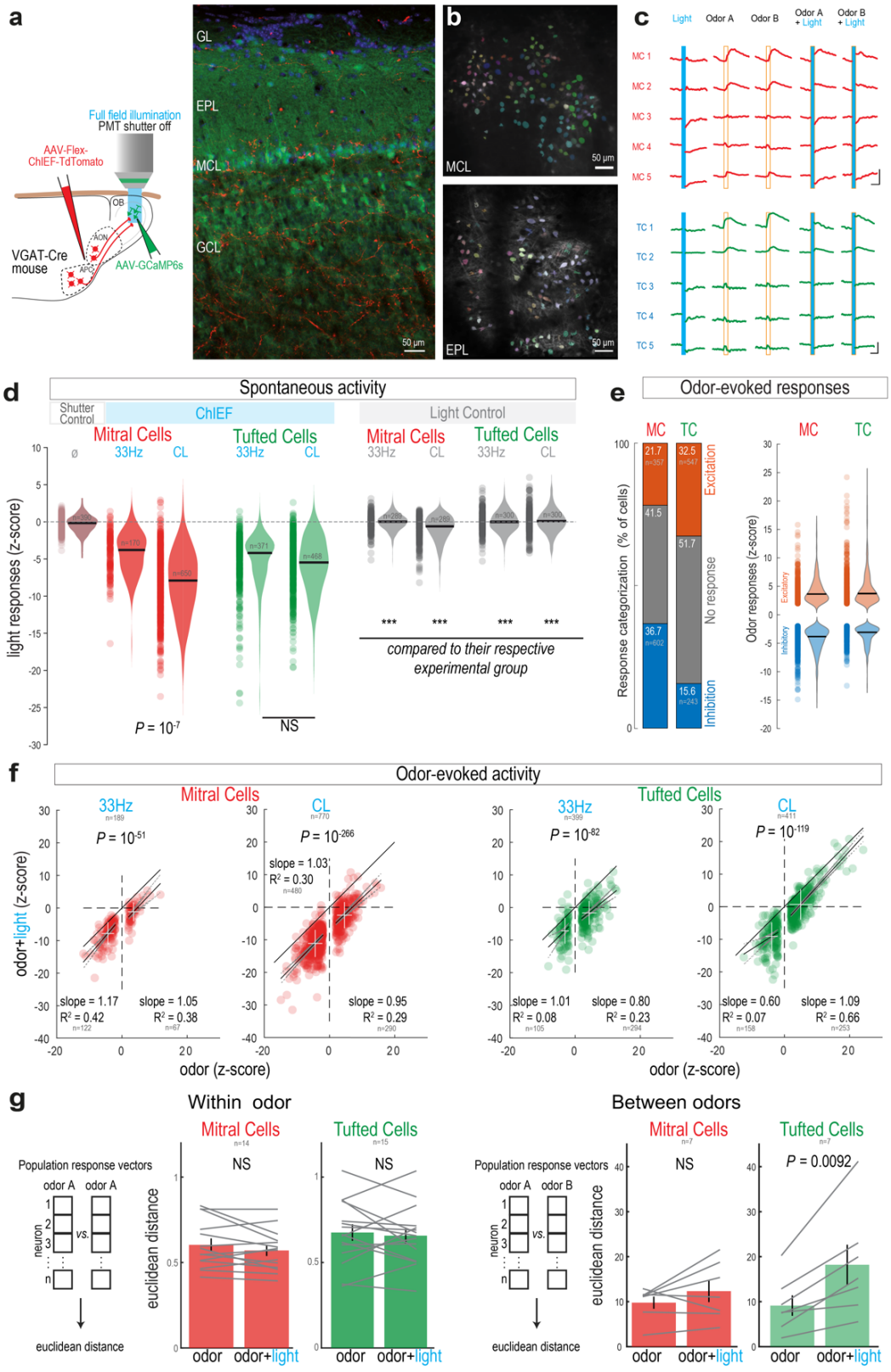

Figure 5. GABAergic feedback axon stimulation inhibits TC and MC activity *in vivo*. a, Two-photon imaging of TC and MC in awake mice coupled to full-field optogenetic stimulation of GABAergic cortical axons

through the microscope objective. Right, Post-hoc confocal image showing the GCaMP6s (green) expression in TCs and MCs along with ChiEF-TdTomato^{+} GABAergic axons (red). Blue, DAPI. **b**, Pseudo-colored masks from MCs and TCs obtained by imaging in the MCL (top) and EPL (bottom). **c**, Example traces of MCs (red, top) and TCs (green, bottom) during light (blue shaded box), odors (orange contoured box), and odor and light simultaneous stimulation (blue shaded and orange contoured box). Scale bars, 5% ΔF/F and 2 s. **d**, Light-induced impact on MCs (red) and TCs (green) spontaneous activity (z-scored) in the presence (left) or absence (control, right) of ChIEF. Light illumination (2sec) was either pulsed (33 Hz) or continuous (CL). Ø: "shutter control": closing/reopening the shutter without light stimulation. Violin plots are estimated ks density from the data. Black line, median; circle, individual cell. Light stimulation of ChIEF^{+} GABAergic cortical axons produced significantly greater inhibition than the respective control stimulation without ChIEF (ANOVA with Tukey's post-hoc test, *** $P << 0.001$). In MCs, but not TCs, ChIEF CL stimulation produced greater inhibition than 33 Hz stimulation (two sided t-test). Note that CL control in MCs is significantly greater than "shutter control" (two sided t-test, $P=0.02$; $P>0.05$ for all other comparisons). **e**, Categorization (left) and magnitude (right) of the odor-evoked responses in MCs and TCs. Data are mean ± sem. **f**, MC (left) and TC (right) responses to simultaneous light and odor stimulation versus odor stimulation only (two sided paired t-test). Circle, individual responsive cell-odor pair. White cross is mean ± s.d. for excitatory and inhibitory odor responses, separately. Solid line: equality line. **g**, In odor responsive neurons, light stimulation did not alter the intra-odor Euclidean distance (distance between the population responses to the same odor; "Within odor). However, In TCs, but not MCs, light stimulation increased the inter-odors Euclidean distance (distance between the population responses to the two odors, "Between odors"; two sided paired t-test).

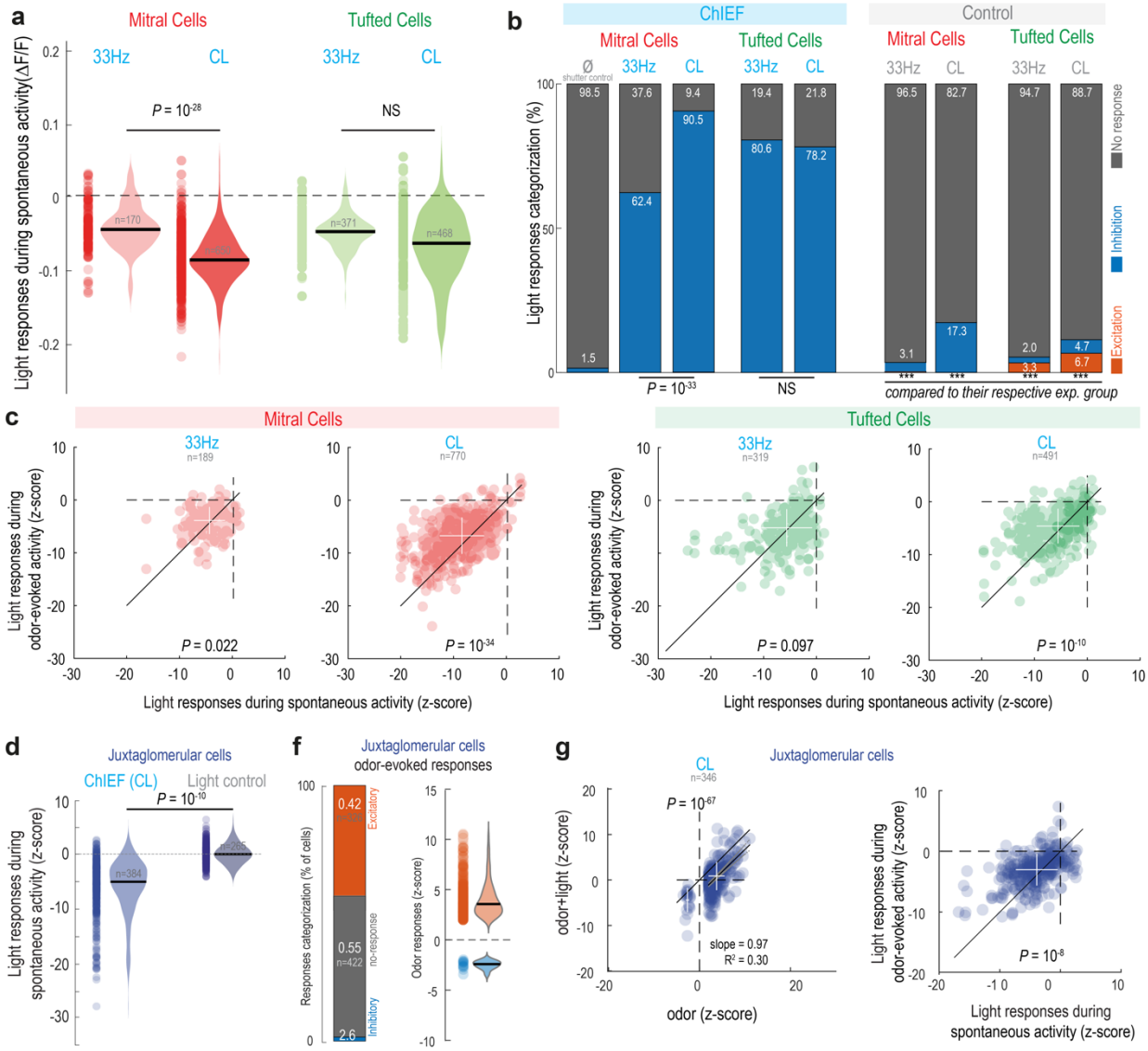

Extended Data Fig. 4. Additional analysis of cortico-bulbar inhibition of OB output neurons. a, ΔF/F0 light responses to 33 Hz and CL for MCs (left) and TCs (right) during spontaneous activity. All experimental groups were significantly higher than their respective light control (two sided t-test, $P << 0.001$ for all comparisons). CL induced greater inhibition than 33 Hz stimulation in MCs, but not TCs (two sided t-test). Violin represents ks-density estimation of the data. Black bar, median; circle, individual cell. n as in Fig. 5d. **b**, Categorization of light responses to optogenetic stimulation (left) and light control (right) for MCs and TCs during spontaneous activity. Light caused significantly more significant inhibition in all experimental groups compared to their respective light control (χ^2 test, $p << 0.001$ for all comparisons). CL produced

significant inhibition in a greater proportion of MCs, but not TCs (χ^2 test). Note that control CL illumination on MCs induced signification inhibition in a sizable proportion of MCs. n as in Fig. 5d. **c**, In odor-responsive MCs (left) and TCs (right), light inhibition of spontaneous activity was slightly stronger than during odor-evoked (two-sided paired t-test). White cross denotes mean ± s.d. n as in Fig. 5f. **d**, CL illumination induced a significant inhibition of JG spontaneous activity (z-scored) in the presence of ChIEF compared to the "light control" (One-way ANOVA with Tukey's post-hoc test, $P = 10^{-10}$). **f**, Categorization (left) and magnitude (right) of the odor-evoked responses in JG cells. (Violins are ks-density estimates of the data. Black bar, median; circles, individual cell-odor pair. **g**, Effect of CL stimulation on odor-evoked responses in JG cells. Left: Odor-responses were significantly dampened upon CL stimulation (paired two sided t-test). Right: Inhibition was slightly greater on spontaneous activity than during odor-evoked (two-sided paired t-test).

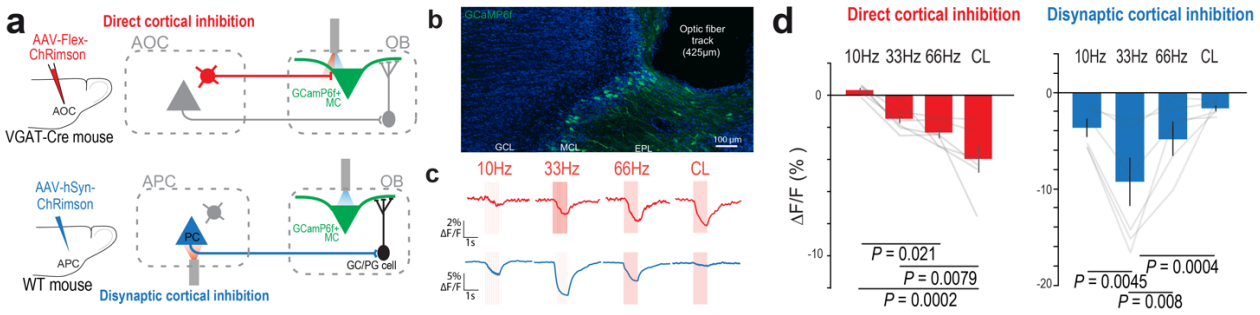

Extended Data Fig. 5. Different frequency-dependent inhibition in direct and disynaptic inhibition. a, MC and TC awake imaging utilizing fiber photometry upon cortical GABAergic axon stimulation ("direct cortical inhibition", red) or APC pyramidal neuron soma stimulation ("disynaptic cortical inhibition", bleu). **b**, Confocal image of GCaMP6f expression in MCs and TCs and optic fiber placed above the lateral MCL and EPL. Blue, DAPI. **c**, Representative average traces of light-evoked inhibitory responses in MC/TC using different stimulation patterns. **d**, Upon stimulation of the cortical GABAergic axons (red, left), CL produced the greatest inhibition (RM-One-way ANOVA with Tukey's post-hoc test, $F(3,15)=12.20$, $P=0.0003$). In contrast, upon stimulation of cortical glutamatergic neurons, 33 Hz produced a greater inhibition than any other stimulation pattern (RM-One-way ANOVA with Tukey's post-hoc test, $F(3,15)=10.89$, $P=0.0005$). Data presented as mean ± sem; Gray, individual recording sites.

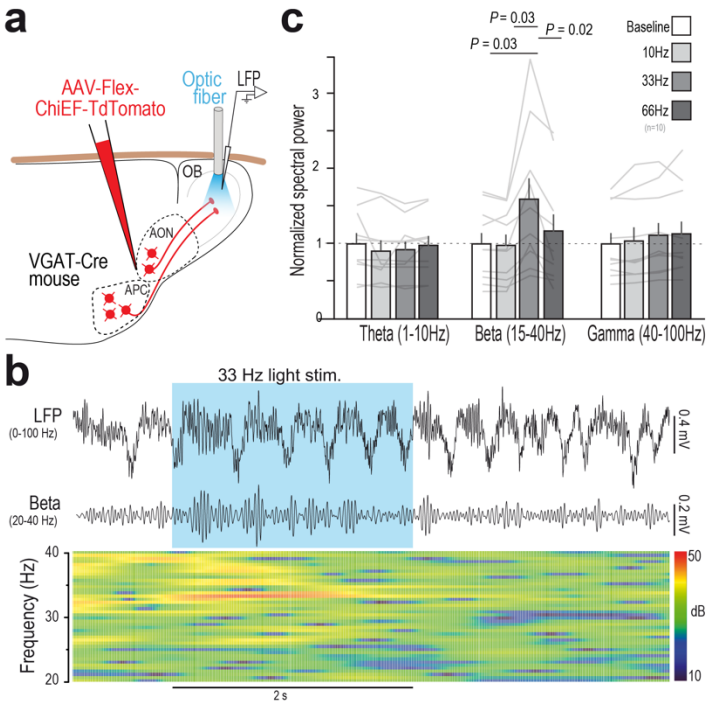

Figure 6. Cortico-bulbar GABAergic axon stimulation increases beta oscillations. a, Awake OB LFP recordings while GABAergic cortical axons were optogenetically stimulated through an optic fiber positioned in the dorsal OB in awake mice. **b**, Example broadband (1-100 Hz, up) and beta-filtered (20-40 Hz, middle) LFP trace recorded in the OB. Blue box: 33 Hz light stimulation (2 s). Bottom, corresponding time-frequency spectrogram of the LFP signal in the beta band. **c**, Quantification of the LFP band power (theta, beta and gamma) during 10 Hz, 33 Hz or 66 Hz stimulation patterns (n = 10 recording sites from 6 mice). Interaction between LFP band and stimulation patterns was significant (repeated measures two-way ANOVA, $F(6,54)=8.08$, $P=10^{-6}$). Within the beta band, 33 Hz stimulation only had a significant effect (repeated measures one-way ANOVA, $F(3,37)=9.875$, $p=0.0054$; Tukey's post-hoc test).

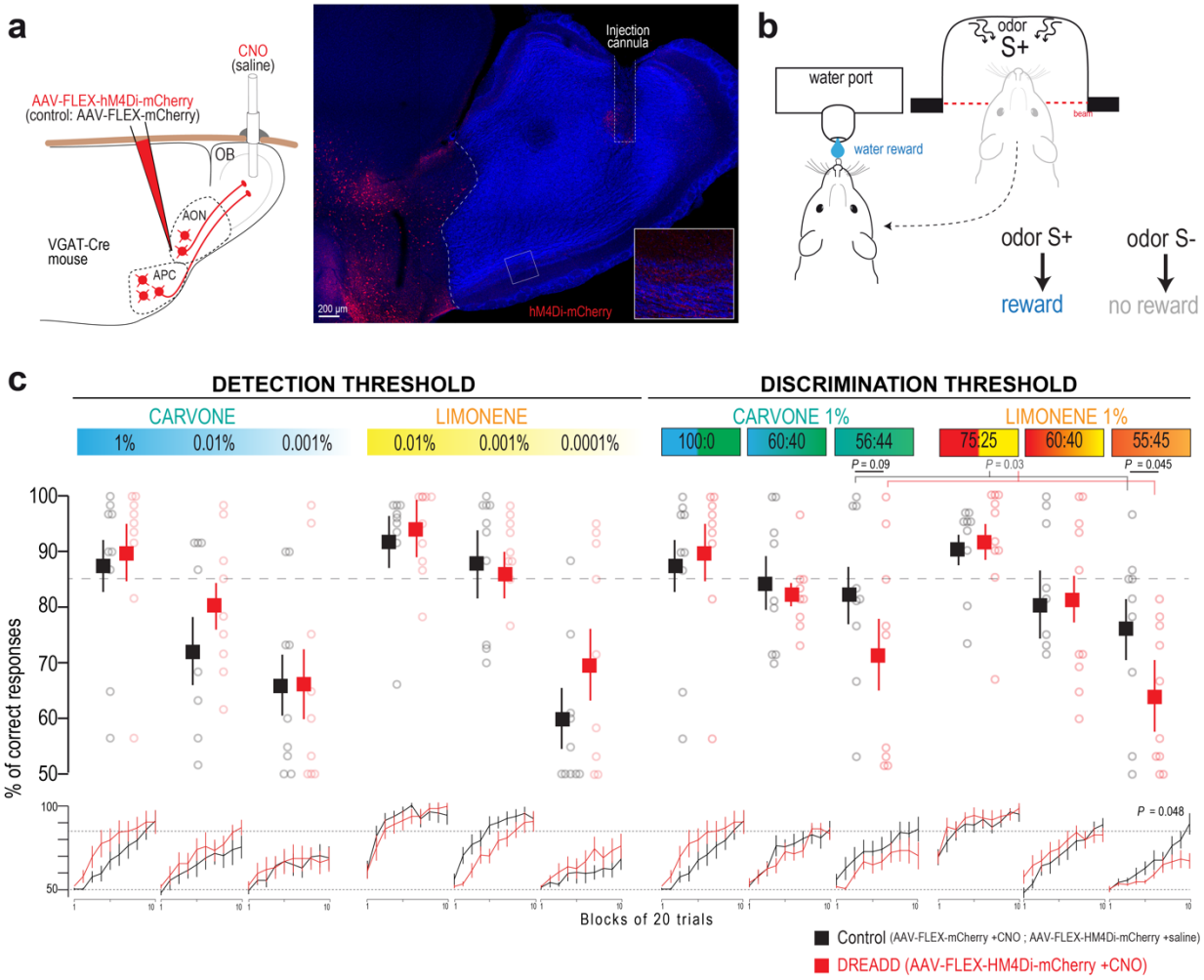

Figure 7. Targeted pharmacogenetic inhibition of cortico-bulbar GABAergic axons impairs fine odor discrimination. **a**, Specific silencing of axonal outputs of AOC GABAergic neuron expressing hM4Di-mCherry by locally injecting CNO in the OB (0.1 mg/mL, 1 µL per hemisphere). Control animal expressed the protein mCherry and also received bilateral CNO injection. Right, Coronal section showing hM4Di-mCherry^{+} GABAergic cells in the AON and their axonal projections in the OB, together with the track of the injection cannula targeted to the core of the OB. Inset: high magnification of the boxed region with increased red fluorescence gain. **b**, Odor-reward association task. After a nose poke into the odor port, mice had to lick on the rewarded odor (S^{+}) to obtain a water reward and refrained licking on the non-rewarded odor (S-). **c**, Performance (percentage of correct responses) for the discrimination of the carvone (green/blue) and limonene (red/yellow) enantiomers. Mean final performance (top; 3 last blocks, i.e. 60

last trials) and mean performance per block of 20 trials (bottom; 10 blocks per session, i.e. 200 trials). CNO reduced the performance for fine limonene mixture discrimination (enantiomers mixtures: 55/45 vs 45/55; top, two-sided Mann-Whitney test; bottom, repeated measure two-way ANOVA, $F(9,153)=1.955$, $P=0.0483$; hM4Di, n = 10 mice; Control, n = 9 mice). A similar trend was observed on carvone enantiomers, although it did not reach significance (n = 9 mice in each group, two-sided Mann-Whitney test). The effects of CNO on fine discrimination performance was still significant when analyzing together carvone and limonene performances (55/45 & 56:44, last three blocks; two-way ANOVA, $F(1,33)=5.115$, $P=0.0304$). Data presented as mean ± sem. Circle, individual mouse. Note that the data for carvone 1% and for carvone 100:0 are the same data.

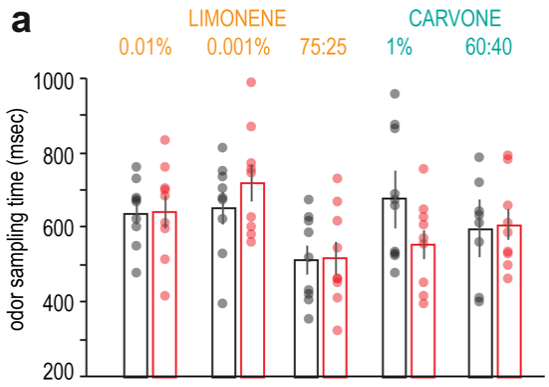

Extended Data Fig. 6. Additional analysis of the behavioral effects of GABAergic cortico-bulbar axon silencing. Mean odor sampling time for sessions with mean performance on the last three blocks superior or equal to the criterion level (85%).

	Rise time Tau		Tau	
	Value (ms)	**n**	**Value (ms)**	**n**
GC	0.40 ± 0.04	17	9.64 ± 1.85	15
dSAC	0.43 ± 0.09	7	10.35 ± 1.77	6
MC	1.05 ± 0.20	8	7.55 ± 1.22	4
eTC	0.70 ± 0.22	8	5.88 ± 2.71	5

Extended Data Table 1. Rise time and tau of the GABAergic responses in different post-synaptic neurons. Data presented as mean ± sem.